



저작자표시-비영리-변경금지 2.0 대한민국

이용자는 아래의 조건을 따르는 경우에 한하여 자유롭게

- 이 저작물을 복제, 배포, 전송, 전시, 공연 및 방송할 수 있습니다.

다음과 같은 조건을 따라야 합니다:



저작자표시. 귀하는 원저작자를 표시하여야 합니다.



비영리. 귀하는 이 저작물을 영리 목적으로 이용할 수 없습니다.



변경금지. 귀하는 이 저작물을 개작, 변형 또는 가공할 수 없습니다.

- 귀하는, 이 저작물의 재이용이나 배포의 경우, 이 저작물에 적용된 이용허락조건을 명확하게 나타내어야 합니다.
- 저작권자로부터 별도의 허가를 받으면 이러한 조건들은 적용되지 않습니다.

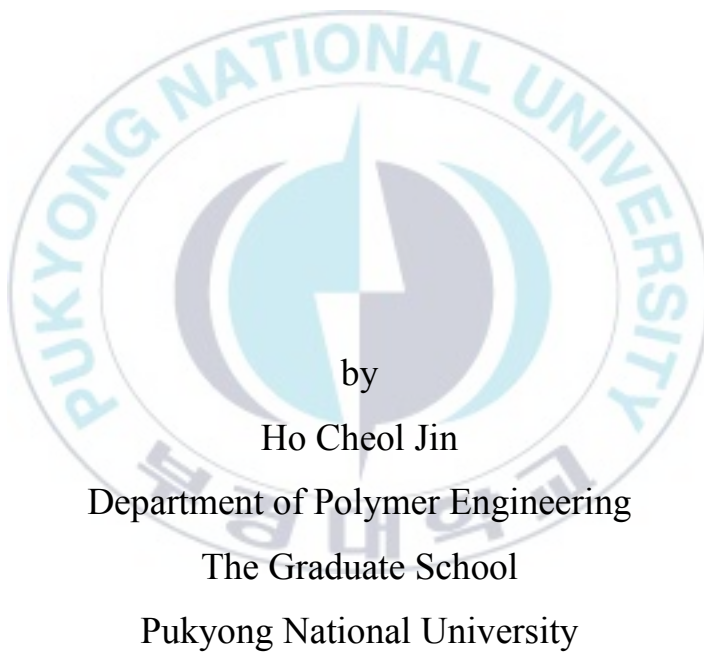
저작권법에 따른 이용자의 권리는 위의 내용에 의하여 영향을 받지 않습니다.

이것은 [이용허락규약\(Legal Code\)](#)을 이해하기 쉽게 요약한 것입니다.

[Disclaimer](#)

Thesis for the Degree of Master of Engineering

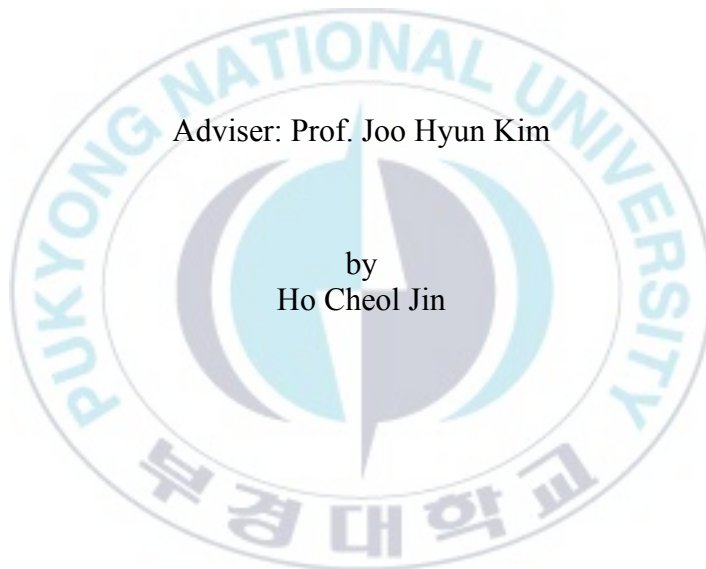
Effect of Diverse Organic Electrolytes as the Cathode Buffer layer on the Photovoltaic Property



February 21, 2020

Effect of Diverse Organic Electrolytes as the Cathode Buffer layer on the Photovoltaic Property

(유기전해질이 음극 버퍼층으로써 고분자 태양전지 특성에 미치는 영향)



Adviser: Prof. Joo Hyun Kim

by
Ho Cheol Jin

A thesis submitted in partial fulfillment of the requirements
for the degree of

Master of Engineering

in Department of Polymer Engineering, The Graduate School,
Pukyong National University

February 21, 2020

Effect of Diverse Organic Electrolytes as the Cathode Buffer layer on the Photovoltaic Property

A dissertation
by
Ho Cheol Jin

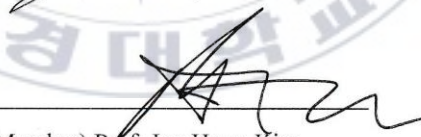
Approved by:



(Chairman) Prof. Seong il Yoo



(Member) Prof. U Hyeok Choi



(Member) Prof. Joo Hyun Kim

February 21, 2020

Contents

Contents.....	i
List of Figures.....	v
List of Tables.....	viii
Abstract.....	ix
 Chapter I Introduction	
I - i Motivation.....	1
I - ii Organic Solar Cells.....	3
I - ii-1. Bulk-Heterojunction (BHJ).....	4
I - ii-2. Metal-semiconductor junction.....	5
I - ii-3. Charge Transport layer (CTL).....	6
I - iii General Parameters of Solar Cells.....	8
I - iii-1. The Equivalent Circuit Diagram (ECD).....	9

I -iii-2. Short Circuit Current (I_{sc}).....	10
I -iii-3. Open Circuit Voltage (V_{oc}).....	11
I -iii-4. Fill Factor (FF).....	12
I -iv Light Intensity Dependence of J_{sc} and V_{oc}	13
I -v Space Charge limited Current (SCLC).....	14
I -vi Abbreviations and Synonyms.....	15
<p>Chapter II New Organic Electrolytes based on Tosylate as the Cathode Buffer Layer</p>	
II- i Introduction.....	16
II- ii Experiment.....	17
II- ii -1. Materials.....	17
II- ii -2. Synthesis.....	18
II- ii -3. Measurement.....	19
II- ii -4. Fabrication of OSCs.....	20
II- iii Results and discussion.....	21

Chapter IV Effect of acid derivatives with conjugated polymer electrolyte as the cathode buffer layer on the photovoltaic property

IV- i Introduction.....	42
IV- ii Experiment.....	44
IV- iii Results and discussion.....	45
IV- iv Conclusion.....	53
References.....	54
Acknowledgement.....	60

List of Figures

Figure I -1 (a) the global average temperature change after 1880 (National Aeronautics and Space Administration Goddard Institute for Space Studies(NASA GISS)) and (b) the carbon dioxide concentration at Mauna Loa Observatory after 1958 (Scripps Institute of Oceanography (SIO)).

Figure I -2 The generation process of photo-induced charges along with the interpenetrating phase-separated D-A network.

Figure I -3 (a) Metal-semiconductor (M-S) junction and heterojunction (HJ) in the OSCs and (b) the induced the energy barrier in M-S junction.

Figure I -4 The variation in energy barrier (a) before and (a) after interfacial dipole induction.

Figure I -5 The typical current(I)-voltage (V) curve in solar cells and the definition of the fill factor (FF).

Figure I -6 The equivalent circuit diagram (ECD) of the OSCs consists of the following ideal components: A current I_L that accounts for the light-generated current, a diode D that considers the nonlinear voltage dependence and a shunt R_{sh} and series resistor R_s . Also shown is a load resistor R_L and its voltage drop V . The current arrows point into the direction the holes flow – according to the standard in electronics. The current I is negative if $V > V_{OC}$ and it flows into the device.

Figure I -7 The classical schematic log-log plot showing the transition from the ohmic current to the SCLS regime as increasing the applied voltage.

Figure II -1 Chemical structures of (a) TEG-M-OTs, V-C12-OTs, PC₇₁BM, and PTB7. Device structures based on (b) ITO and (c) ITO/ZnO.

Figure II -2 Current-voltage curves of OSCs under AM 1.5G simulated illumination with an intensity of 100 mW/cm² (insert: in the dark

condition; square: ZnO/MeOH, circle: TEG-M-OTs, triangle: V-C12-OTs) (a) with ZnO, and (b) without ZnO.

Figure II -3 The energy level diagram of the device based on (a) ITO/ZnO, (b) ITO.

FigureIII-1 Current density–voltage curves of OSCs ZnO, ZnO/V-alkyl-OTs under illumination (inset: in the dark condition) in this research.

FigureIII-2 ^1H NMR, ^{13}C NMR and electrospray ionization (ESI)-MASS spectra of V-alkyl-OTs; (a)-(c) C4, (d)-(f) C6, (g)-(i) C12.

FigureIII-3 (a) XPS survey spectra and (b) Zn 2p spectra of ZnO with and without V-alkyl-OTs.

FigureIII-4 AFM images, the average roughness (R_a) and static water contact angle of ZnO, ZnO/V-C4-OTs, ZnO/V-C6-OTs, ZnO/V-C12-OTs.

FigureIII-5 (a) Current density–voltage curves of OSCs ZnO, ZnO/V-alkyl-OTs under illumination (inset: in the dark condition) and (b) the work function of ZnO/V-alkyl-OTs and the energy diagram of the device in this research.

FigureIII-6 (a) Current density–voltage curves of the electron-only device with a configuration of ITO/ZnO(25nm) with or without V-alkyl-OTs/PC₇₁BM(60nm)/Al(100nm). (inset: with fitted line, V: applied voltage, V_{bi} : built-in voltage, V_{on} : turn-on voltage) and (b) impedance spectra of the OSCs based on ZnO without and with V-alkyl-OTs.

FigureIII-7 Photo-generated current density (J_{ph}) and (b) the carrier transporting and collecting probability vs. effective voltage (V_{eff}) plots of the OSCs.

FigureIV-1 Chemical structure of (a) PFN with diverse acid derivatives, (b) PTB7-Th and PC₇₁BM, and (c) the device structure of OSC used in this study.

FigureIV-2 (a) XPS survey spectra, (b) F 1s, and (c) S 2p spectra of ZnO and PFN-acids coated ZnO.

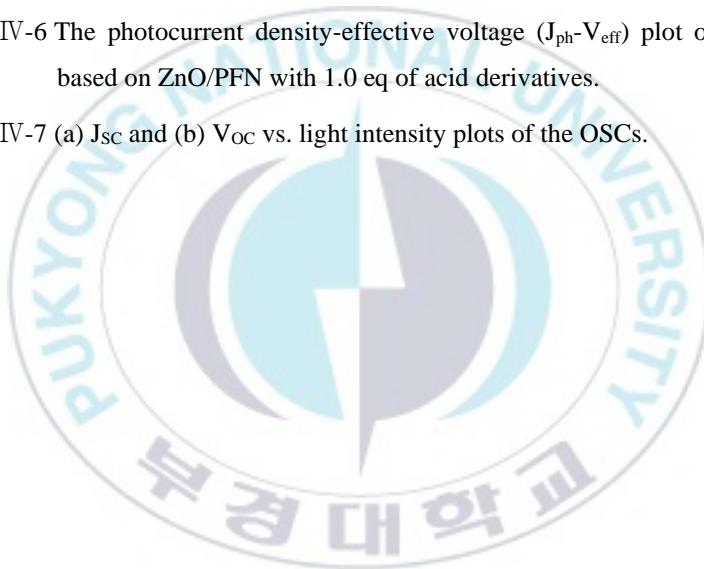
FigureIV-3 The reaction between PFN and acid derivatives.

FigureIV-4 AFM images and the average roughness (Ra) of ZnO/PFN with (a) 1.0 eq and (b) 6.0 eq of CF₃AA.

FigureIV-5 (a) Current density–voltage curves under illumination (inset: under dark conditions) and (b) EIS spectra of OSCs based on ZnO and ZnO/PFN with 1.0 eq of acid derivatives.

FigureIV-6 The photocurrent density-effective voltage (J_{ph} - V_{eff}) plot of OSCs based on ZnO/PFN with 1.0 eq of acid derivatives.

FigureIV-7 (a) J_{sc} and (b) V_{oc} vs. light intensity plots of the OSCs.



List of Tables

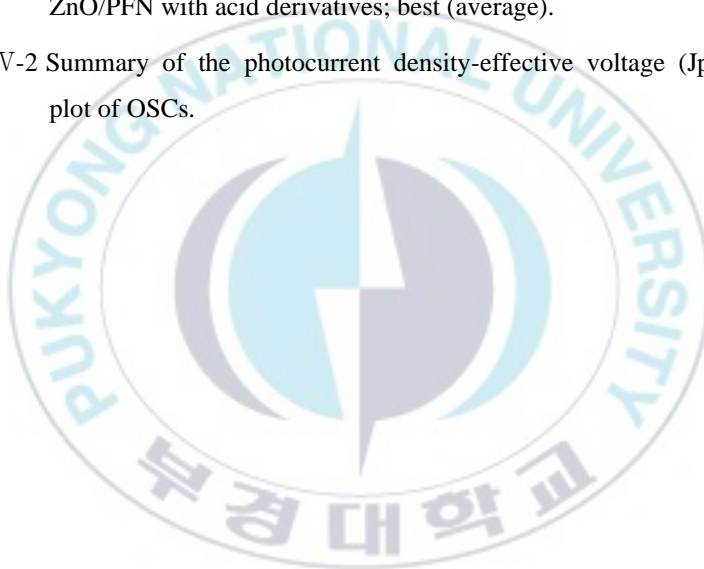
Table I -1. List of common abbreviations used throughout the thesis.

Table II -1 Summary of photovoltaic parameters of OSCs based on ZnO, ITO/TEG-M-OTs, and ITO/V-C12-OTs; best (average).

TableIII-1 Summary of photovoltaic parameters of OSCs based on ZnO, ITO/V-alkyl-OTs; best (average).

TableIV-1 Summary of photovoltaic parameters of OSCs based on ZnO and ZnO/PFN with acid derivatives; best (average).

TableIV-2 Summary of the photocurrent density-effective voltage (J_{ph} - V_{eff}) plot of OSCs.



유기전해질이 음극 버퍼층으로써 고분자 태양전지 특성에 미치는 영향

진 호 철

부 경 대 학 교 대 학 원 고 분 자 공 학 과

요 약

화석 연료의 고갈과 환경 문제에 따라 재생 에너지의 개발이 세계적 흐름으로 자리 잡고 있다. 그 중 태양광 발전은 별다른 기계적 장치 없이 태양광을 직접 전기로 변환할 수 있어, 오늘날 점점 더 중요한 에너지원으로 꼽히고 있다. 이 중 유기태양전지는 투명하고 유연한 성질을 가지고 있어 다양한 공간, 장소에 적용 가능하고 무게가 가벼워 휴대하기도 용이하다. 게다가 용액 공정으로 제작할 수 있어 제작 단가도 상당히 저렴하다. 하지만 여전히 낮은 효율과 안정성 등으로 상용화되기에는 제약이 있다.

보통 유기태양전지의 구조는 유리/인듐-주석 산화물(ITO)/산화아연(ZnO)/유기 광활성층/은(Ag)로 구성되는데, 이는 무기물인 ZnO 층 위에 유기물인 광활성층이 코팅된 구조이다. 따라서, 두 층은 서로 상반된 성질을 가져 박막 간에 상호작용을 원활하게 이루어지지 않게 만든다. 이는 두 층 사이에 계면을 개질하여 해결할 수 있다. 그 개질제로 이온성 유기물이 많이 사용되는데, ZnO 층에 표면 쌍극자를 유도하여 반도체 접합간 생기는 에너지 장벽을 줄이기 위함이다. 이에 본 논문에서는 V-alkyl-OTs와 TEG-M-OTs라는 tosylate계 유기저분자를 설계 및 합성하여 메탄올을 용매로 ZnO 층과 유기 광활성층 사이에 스핀 코팅하였다. 일함수를 측정한 결과 V-OTs와 TEG-OTs가 코팅된 ZnO 층의 일함수는 ZnO 층 (기준소자)에 비해 감소하였다. 이는 V-alkyl-OTs와 TEG-M-OTs에 있는 quaternary ammonium tosylate와 hydroxyl group에 의해 형성된 interface

dipole에 의해 기인했다. 그 결과, 소자의 전류가 상승하여, 효율이 ZnO 소자(Ref 7.48%)에 비해 V-alkyl-OTs 소자는 8.62%, TEG-M-OTs 소자는 7.74%로 상승하였다.

Polymer에 대한 연구도 진행하였는데, PFN이라는 이미 유명한 물질을 이용하였다. 기존의 PFN은 초산(AA)과 함께 메탄올에 녹여 PFN-AA 형태로 이용하고 있는데, 이에 본 논문에서는 초산보다 더 강한 쌍극자를 가진 p-Toluenesulfonic acid (TsOH)를 이용하여 PFN-OTs 형태로 ZnO 표면에 적용하였다. 그 결과, PFN-AA 소자(Ref. 9.75%)에 비해 PFN-OTs 소자는 10.55%까지 그 효율이 상승했다.



Chapter I

Introduction

I - i Motivation

The issues of the existing main energy sources (oil, coal, and uranium) have a way of coming to the surface, such as the environment effect and potential risk. Especially, after it has been demonstrated that the greenhouse effect of carbon dioxide (CO_2) from human activities can increase the global average temperature,^[1, 2] the excessive greenhouse effects are really occurring today due to rapid increase of CO_2 in atmosphere (**Fig. I -1(a), (b)**). These CO_2 concentration uptrend for the last 100 years is unusual compared with the last 160,000 years. Please note that the CO_2 concentration never once exceeded 300 parts per million (ppm) except for the last 100 years.^[3]

Recently, the CO_2 concentration is over 400 ppm and the accumulation rate is not a range that can be solved by the earth's self-purification. In 2014, Intergovernmental Panel on Climate Change (IPCC) reported that the greenhouse effect increased the global mean surface temperature by 0.85°C for the year 1880 – 2012 and the global sea level by 0.19cm for the year 1901-2010.^[4] Even if the global net emissions of artificial CO_2 Converge with zero, the global mean surface temperature will continue to keep the recent increase level.^[4] Thus, we must have an effort to decrease the emission and concentration of CO_2 .

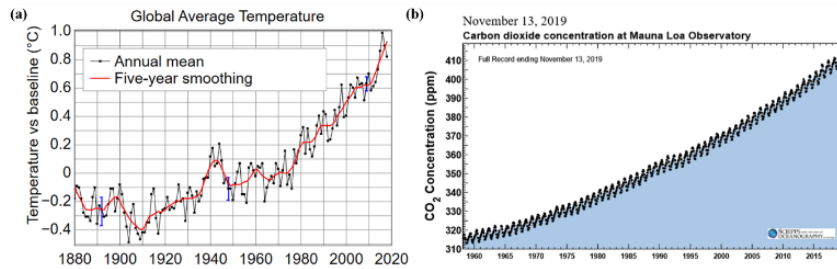


Figure I - 1 (a) the global average temperature change after 1880 (National Aeronautics and Space Administration Goddard Institute for Space Studies(NASA GISS)) and (b) the carbon dioxide concentration at Mauna Loa Observatory after 1958 (Scripps Institute of Oceanography (SIO)).

The worldwide efforts for CO₂ reduction are ongoing in two ways, the CO₂ emission reduction and CO₂ fixation. Fortunately, we already have the harvesting technologies for many renewable energy sources which no generate CO₂, such as wind, tidal, geothermal, hydrogen, solar energy. It is important to know that they can supply more energy compared with the consumed energy for the fabrication, installation, and maintenance of their power system. Despite of obvious merits, the affordability and efficiency yet remain the obstacles to their commercialization. If we can not soon develop affordable harvesting technologies for renewable energy sources, we should hope that the costs of environmental hazards of existing power sources excess them of the fabrication, installation, and maintenance of future power systems.

I - ii **Organic Solar Cells**

At present, various types of solar cells were designed with the development of new semiconductor materials such as inorganic, dye-sensitized, organic, and quantum dots solar cells. Of course, each has pros and cons and the researches are ongoing for the breakthrough of the weakness. The organic solar cells (OSCs) among them have the outstanding merits of structural diversity and fabrication process due to the organic material base.



I - ii -1. Bulk-Heterojunction (BHJ)

The OSCs was not promising in a field dominated by inorganic materials due to the low power conversion efficiency (PCE) of $< 0.1\%$. The main issue was in the exciton dissociation process. The OSCs needed to give the sufficient electric field to split excitons and the way in overcoming the short diffusion length of excitons ($\sim 10\text{nm}$). To resolve these problems, the BHJ solar cells featuring donor-acceptor (D-A) blend layer were first suggested in 1995.^[5] The basic concepts of the BHJ are to overcome, first, the insufficient electric field through the fast photoinduced electron transfer between the polymer and the fullerene derivative, and second, the limited diffusion length ($\sim 10\text{ nm}$) through the interpenetrating phase-separated D-A network (**Fig. I - 2**).

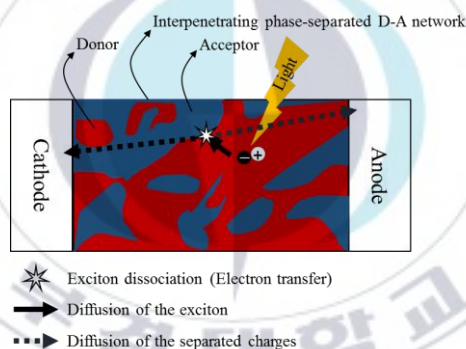


Figure I - 2 The generation process of photo-induced charges along with the interpenetrating phase-separated D-A network.

After the development of BHJ solar cells, even for 24 years, the basic structure of BHJ solar cells has been kept intact, and there were the much further improvements in the PCEs from optimization of the charge transfer and transport properties by the blend composition,^[6, 7, 8] the network morphology,^[9, 10] and charge transport layer,^[11] etc. Recently, the PCEs of the BHJ solar cells reached 17%.^[12]

I - ii -2. Metal-semiconductor junction

Metal-semiconductor (M-S) junction and heterojunction (HJ) inducing the energy barrier exist in the OSCs (**Fig. I - 3(a), (b)**). While the energy barrier of the HJ supplies the energy for exciton dissociation as mentioned before, that of the M-S junction hinders charge transfer from D or A to each electrode. It is because the energy barrier height induced by the M-S junction, called “a Schottky barrier height”, decides whether rectifying or ohmic contact. The Schottky barrier height can be predicted roughly by Schottky–Mott rule:

$$\Phi_B^{(n) \text{ or } (p)} \approx \Phi_{\text{metal}} - \chi_{\text{semi}}^{\text{EA or IP}} \quad (\text{I -1})$$

where $\Phi_B^{(n) \text{ or } (p)}$ is the Schottky barrier height of the M-S junction with n- or p-type semiconductor and Φ_{metal} is the work function of metal and $\chi_{\text{semi}}^{\text{EA or IP}}$ is the electron affinity (EA) or ionization potential (IP) of the semiconductor. In practice, the junction of ITO/[6,6]-Phenyl C71 butyric acid methyl ester (PC₇₁BM), usually used as transparent electron and acceptor, shows the $\Phi_B^{(n)}$ of ~1eV, which means that this junction is a rectifying contact. Thus, the charge transport layer (CTL) is inserted between a photoactive layer and electrodes to reduce the Schottky barrier and induce the ohmic contact.

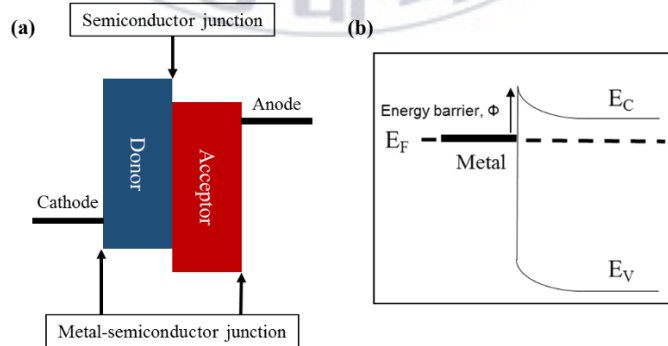


Figure I - 3 (a) Metal-semiconductor (M-S) junction and heterojunction (HJ) in the OSCs and (b) the induced the energy barrier in M-S junction.

I - ii -3. Charge Transport Layer (CTL)

The metal oxide or polymer is usually used as the CTL in the OSCs. The first requirement of CTL materials is to have the proper electron affinity (EA) and ionization potential (IP). In other words, the appropriate highest occupied molecular orbital (HOMO) and lowest unoccupied molecular orbital (LUMO) are prerequisites of CTL materials. In practice, the zinc oxide (ZnO), the representative electron transport layer (ETL) material, has the HOMO of $\sim 4.4\text{eV}$ which is lying between the work function of the cathode and the LUMO of acceptor material. In the case of hole transport layer (HTL) material, the poly(3,4-ethylenedioxythiophene):poly(styrenesulfonate) PEDOT:PSS also has the LUMO of $\sim 5.2\text{eV}$ which is lying between the work function of anode and the HOMO of donor material.

Although the CTL reduced the Schottky barrier between electrodes and the photoactive layer, there is room for further improvement due to a new semiconductor junction on the CTL interface. Especially, the modification of the ZnO interface is being studied to reduce the energy barrier by conjugated/non-conjugated electrolytes^[13-15] or metal ingredients^[16, 17]. The main concept of this researches is that the interfacial dipole induced by electrolytes can reduce the energy barrier. (Fig. I - 4)

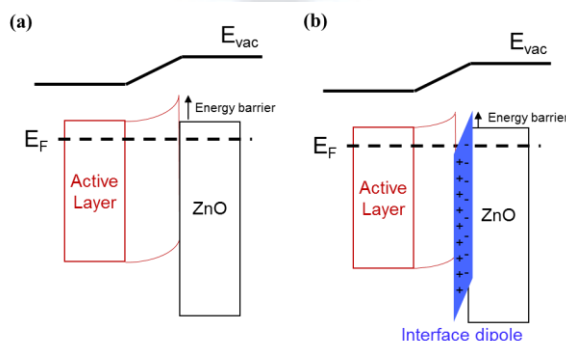


Figure I - 4 The variation in energy barrier (a) before and (a) after interfacial dipole induction.

In this thesis, we report tosylate-based organic electrolytes as ZnO interface modifier of OSCs in chapters 2, 3, 4. Two electrolytes with non-conjugated/conjugated core are compared in Chapter 2. Then, Chapter 3 shows how three electrolytes with different alkyl chain lengths affect to the PCE of OSCs. Finally, in chapter 4, we apply the conjugated polymer electrolyte with diverse acid derivatives as a ZnO interface modifier.



I -iii General Parameters of Solar Cells

The most important parameter of solar cells may be the power conversion efficiency (PCE). The PCE is defined as follows:

$$\eta \equiv \frac{P_{max}}{P_{in}} \quad (I-2)$$

where η is the PCE and P_{max} is the generated power on maximum point and P_{in} is the power of the incident beam. Then, we can easily calculate the P_{max} from this I-V curve. In **Fig. I - 5**, the P_{max} corresponds with the filled rectangle area and the area can not exceed the dotted rectangle area. Then, the fill factor (FF) is defined as the ratio of the filled area to the dotted area as written in Fig. 5.

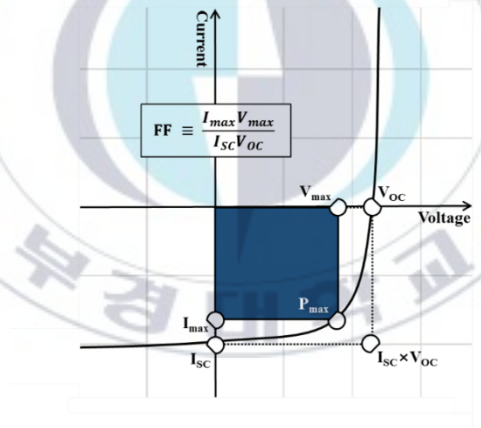


Figure I - 5 The typical current(I)-voltage (V) curve in solar cells and the definition of the fill factor (FF).

Finally, the PCE can be calculated by the following equation:

$$\eta = \frac{I_{sc} \times V_{oc} \times FF}{P_{in}} \quad (I-3)$$

where I_{sc} is the short circuit current and V_{oc} is the open circuit voltage. Then, we should understand the meaning of each value, I_{sc} , V_{oc} , and FF.

I - iii -1. The Equivalent Circuit Diagram (ECD)

The characteristics of the I-V curve can be evaluated through the ECD. The Fig. 6 below is the ECD typically used for solar cells.

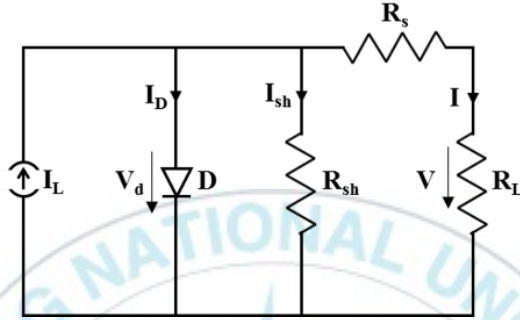


Figure I - 6 The equivalent circuit diagram (ECD) of the OSCs consist of the following ideal components: A current I_L that accounts for the light-generated current, a diode D that considers the nonlinear voltage dependence and a shunt R_{sh} and series resistor R_s . Also shown is a load resistor R_L and its voltage drop V . The current arrows point into the direction the holes flow – according to the standard in electronics. The current I is negative if $V > V_{OC}$ and it flows into the device.

Based on the ECD of solar cells, we can formulate the following equation:

$$(I_L - I_D - I)R_{sh} = V + IR_s \quad (I - 4)$$

Then, using the Shockley diode equation, this can be transformed into

$$I = \frac{I_L - \frac{V}{R_{sh}}}{1 + \frac{R_s}{R_{sh}}} - \frac{I_0}{1 + \frac{R_s}{R_{sh}}} \left(e^{\frac{V - IR_s}{nV_T}} - 1 \right) \quad (I - 5)$$

where I_0 is the reverse bias saturation current and V_T is the thermal voltage and n is the ideality factor. We can get the further discussion of the parameters of solar cells from this equation.

I -iii -2. The Short Circuit Current (I_{SC})

The I_{SC} is the current of solar cells at $V = 0$. Thus, we can easily derive the I_{SC} from Eq. (I -5) as the following equation:

$$I_{SC} = (1 - \frac{R_s}{R_{sh}})\{I_L - I_0 \left(e^{\frac{IR_s}{nVT}} - 1 \right)\} \quad (I -6)$$

This equation shows three terms to get high I_{SC} ; (1) high I_L , (2) $\frac{R_s}{R_{sh}} \approx 0$, and (3) low I_0 . The terms are related to the photo-generated current, loss current, and energy barrier, respectively. In detail, we can get high I_{SC} by expanding the absorption coverage of the photoactive materials for the high I_L or reduce the loss current and energy barrier by optimizing the charge transfer and transport process. Thus, the I_{SC} in this thesis can be enhanced by reducing the loss of the Schottky barrier height, as mentioned before.

I -iii-3. The Open Circuit Voltage (V_{OC})

The V_{OC} is the voltage of solar cells at $I = 0$. Then, we can assume R_s is 0 because there is no current. Thus, we can easily derive the V_{OC} from Eq. (1.5) as the following equation:

$$V_{oc} = nV_T \ln\left(\frac{I_L - V_{OC}/R_{sh}}{I_0} + 1\right) \quad (I-7)$$

Then, assuming $\frac{I_L - V_{OC}/R_{sh}}{I_0} + 1 \approx \frac{I_{sc}}{I_0}$, this can be transformed into

$$V_{oc} \approx nV_T \ln\left(\frac{I_{sc}}{I_0}\right) \quad (I-8)$$

However, this equation can not adopt in the OSCs system because there is not a term related to the difference between the HOMO of donor and LUMO of acceptor (ΔE_{HL}). In this regard, the effective barrier height (φ_b) can be introduced^[18]

$$V_{oc} \approx \frac{n}{q} \varphi_b - nV_T \ln\left(\frac{I_{00}}{I_{sc}}\right) \quad (I-9)$$

where q is an elementary charge and I_{00} is prefactor of I_0 in a thermally activated injection expression, $I_0 = I_{00} e^{\frac{\varphi_b}{kT}}$. This equation predicts the V_{OC} reasonably by setting $\varphi_b = \frac{\Delta E_{HL}}{n'}$.

$$V_{oc} \approx \frac{n}{n'} \Delta E_{HL} - nV_T \ln\left(\frac{I_{00}}{I_{sc}}\right) \quad (I-10)$$

where n' is the ideality factor adjusting ΔE_{HL} . Although the effect of the modified electrode by the CTL on the V_{OC} was adopted clearly on the same principle^[19, 20], that of the modified CTL by the electrolyte on the V_{OC} was not observed in this thesis.

I -iii -4. Fill Factor (FF)

The last term defining the overall behavior of a solar cell is the fill factor (FF). This is defined by the following expression.

$$FF \equiv \frac{I_{max} \times V_{max}}{I_{sc} \times V_{oc}} \quad (I -11)$$

The FF can be represented by the ratio of the different rectangular areas, as mentioned before. Meanwhile, the R_s and R_{sh} are derived by the inverse slope around 0V and at a $V > V_{oc}$ in **Fig. I -5**, respectively.

$$R_s \approx \left(\frac{I}{V}\right)^{-1}, \text{ at } V > V_{oc} \quad (I -12)$$

$$R_{sh} \approx \left(\frac{I}{V}\right)^{-1}, \text{ at } V = 0 \quad (I -13)$$

Thus, the high R_{sh} and the low R_s lead to the high FF, thus resulting in greater PCE. In other words, the FF shows the ideal value of 1 when the R_{sh} and R_s have the values of ∞ and 0, respectively.

I - iv The Light Intensity Dependence of J_{sc} and V_{oc}

Analysis of the charge recombination mechanism is important because it can show which problem exists in the OSCs. One of the simple methods to analyze the charge recombination mechanism is to measure the short circuit current density (J_{sc}) and V_{oc} along with the light intensity. In practice, the J_{sc} and V_{oc} are decreased as reducing the light intensity, according to the following proportional expression:

$$J_{sc} \propto P^\alpha \quad (I-14)$$

$$V_{oc} \propto nV_T \ln(P) \quad (I-15)$$

where P is the light intensity. The main factor for analysis of the charge recombination is α and n . α mostly has the value from 0.5 to 1 and n does from 1 to 2. These values are determined by whether the recombination process is dominant.

We can analyze the degree of dominance between the mono- and bi-molecular recombination in OSCs from α . The monomolecular recombination is generally referred to as the recombination when the rate depends only on one free carrier (e.g. geminate recombination and trap-assistant recombination). In contrast, if the rate depends on two free carriers (e.g. band-to-band recombination), the recombination is mentioned as the bimolecular recombination. Thus, if there is only a monomolecular recombination process, the I_{sc} is linearly proportional linearly to the P . In vice versa, the I_{sc} is proportional to the square root of the P .

n explains the deviation from the ideal diode behavior and commonly has a value from 1 (ideal) to 2. As the value is approaching 2, trap-assistant recombination becomes dominant because there are no traps in the ideal diode.

I - v Space Charge Limited Current (SCLC)

The excess charge carriers can build up the space charge in the device due to low charge carrier mobilities of semiconductors. Then, the accumulated space charge generates a reverse electric field compared with applied voltage and leads to limited current. This phenomenon is called as the SCLC, which make it possible to calculate the charge carrier mobilities. The SCLC is expressed by:

$$I = qp_0\mu\frac{V}{d} + \frac{9}{8}\epsilon\mu\frac{V^2}{d^3} \quad (I-16)$$

q is the elementary charge, p_0 is the density of the thermally generated free carriers, μ is the mobility, d is the semiconductor thickness, ϵ the dielectric constant of the semiconductor. In the equation, there are two terms, which mean ohmic current ($I \propto V$) and SCLC ($I \propto V^2$), respectively. Thus, the dependence of current transitions from the ohmic current to the SCLC regime as increasing the applied voltage (Fig. 7).

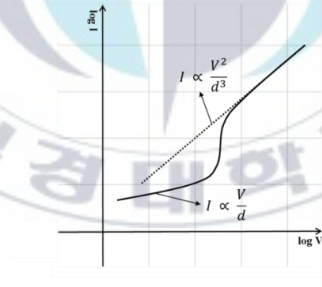


Figure I -7 The classical schematic log-log plot showing the transition from the ohmic current to the SCLC regime as increasing the applied voltage.

On the SCLC regime, the equation can be transformed into

$$I = \frac{9}{8}\epsilon\mu\frac{V^2}{d^3} \quad (1.17)$$

Then, we can calculate the charge mobility from the slope of the $\log(I)$ - $\log(V)$ plot.

I - vi Abbreviations and Synonyms

Table I - 1 List of common abbreviations used throughout the Thesis.

A	Electron acceptor
AFM	Atomic force microscopy
CTL	Charge transport layer
D	Electron donor
ECD	Equivalent circuit diagram
ESI-MASS	Electrospray ionization mass spectrometry
ETL	Electron transport layers
FF	Fill factor
HOMO	Highest occupied molecular orbital
IPCE	Incident photon to current efficiency
I_{ph}	Photo-generated current
I_{sc}	Short circuit current
ITO	Indium tin oxide
J_{ph}	Photo-generated current density
J_{sc}	Short circuit current density
KPM	Kelvin probe microscopy
LUMO	Lowest unoccupied molecular orbital
PC ₇₁ BM	[6,6]-phenyl C71 butyric acid methyl ester
PCE	Power conversion efficiency
PFN	Poly[(9,9-bis(3'-(N,N-dimethylamino)propyl)-2,7-fluorene)-alt-2,7-(9,9-dioctylfluorene)]
PTB7	Poly({4,8-bis[(2-ethylhexyl)oxy]benzo[1,2-b:4,5-b']dithiophene-2,6-diyl} {3-fluoro-2-[(2-ethylhexyl)carbonyl]thieno[3,4-b]thiophenediyl})
PTB7-Th	Poly([2,6'-4,8-di(5-ethylhexylthienyl)benzo[1,2-b:3,3-b']dithiophene] {3-fluoro-2[(2-ethylhexyl)carbonyl]thieno[3,4-b]thiophenediyl})
V_{eff}	Effective voltage
V_{oc}	Open circuit voltage

Chapter II

New Organic Electrolytes based on Tosylate as the Cathode Buffer Layer

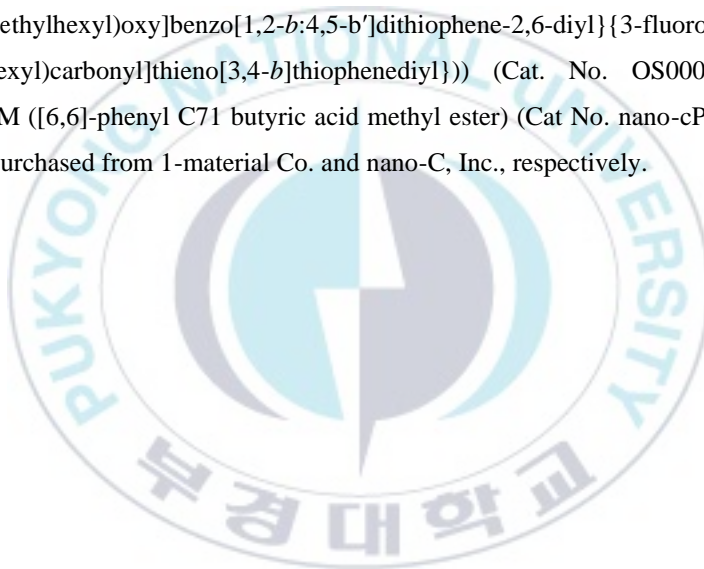
II - i Introduction

Herein, new SM organic electrolytes with two bulky tosylate anions, 2,2'-(ethane-1,2-diylbis(oxy))bis(N,N,N-trimethylethanaminium) benzenesulfonate (**TEG-M-OTs**) and 1,1'-bis(1-dodecyl)-4,4'-bipyridine-1,1'-dium benzenesulfonate (**V-C12-OTs**), were synthesized by the simple quaternization reaction and the addition of **TEG-M-OTs** and **V-C12-OTs** between the ZnO and the active layer improved the PCE of the device from 7.48% to 7.74% and 7.88%, respectively. Although there is no observable change in the open circuit voltage (V_{oc}) of the device with SM electrolytes compared with that of the reference device, the obvious changes in the short circuit current density (J_{sc}) and fill factor (FF) were observed. In addition, the device with **TEG-M-OTs** and **V-C12-OTs** layer without the ZnO leads to the PCE of 4.22 and 6.95%, respectively. It should be noted that the PCE of the device based on **V-C12-OTs** is close to the PCE of the device based on ZnO/MeOH (7.48%) without any calcination.

II - ii Experiment

II - ii -1. Materials

All chemicals were purchased from Alfa Aesar or Sigma-Aldrich and used as received unless otherwise described. 1,2-Ethanedithiolbis(oxy-2,1-ethanediyl) bis(4-methylbenzenesulfonate) (TEG-OTs) and Dodecyl 4-methylbenzenesulfonate (C12-OTs) was synthesized similarly to a previously reported method by Debra L. Mohler and Gang Shen.^[21] PTB7 (Poly({4,8-bis[(2-ethylhexyl)oxy]benzo[1,2-*b*:4,5-*b'*]dithiophene-2,6-diyl}{3-fluoro-2-[(2-ethylhexyl)carbonyl]thieno[3,4-*b*]thiophenediyl})) (Cat. No. OS0007) and PC₇₁BM ([6,6]-phenyl C₇₁ butyric acid methyl ester) (Cat No. nano-cPdM-SF) were purchased from 1-material Co. and nano-C, Inc., respectively.



II - ii -2. Synthesis

2,2'-(ethane-1,2-diylbis(oxy))bis(N,N,N-trimethylethanaminium)

benzenesulfonate (TEG-M-OTs). A mixture of TEG-OTs (1.829 g, 4.00 mmol) and Trimethylamine in Tetrahydrofuran (THF) (1 M, 9.00 ml, 9.00 mmol) was stirred at room temperature for 3 days. The precipitates were filtered and thoroughly washed with THF. The yield of transparent wax-like solid was 66.3% (1.530 g). ¹H NMR (600 MHz, CD₃OD, ppm): 7.71~7.67 (d, J = 8.2 Hz, 4H), 7.25~7.21 (d, J = 8.3 Hz, 4H), 3.92~3.90 (m, 4H), 3.72~3.68 (t, J = 6.2 Hz, 4H), 3.59~3.53 (t, J = 4.8 Hz, 4H), 3.20~3.14 (s, 18H), 2.35~2.32 (s, 6H).

1,1'-bis(1-dodecyl)-4,4'-bipyridine-1,1'-diium benzenesulfonate (V-C12-OTs). A mixture of C12-OTs (1.632 g, 5.00 mmol) and 4,4'-bipyridine (0.312 g, 2.00 mmol) in acetonitrile was stirred at room temperature for 3 days. White precipitates were filtered and washed with acetonitrile. The yield of white solid was 73.4% (1.229 g). ¹H NMR (600 MHz, CD₃OD, ppm): 9.25~9.24 (d, J = 6.2 Hz, 4H), 8.64~8.63 (d, J = 6.2 Hz, 4H), 7.67~7.66 (d, J = 8.3 Hz, 4H), 7.21~7.20 (d, J = 7.5 Hz, 4H), 4.72~4.69 (t, J = 7.55 Hz, 4H), 2.35~2.33 (s, 6H), 2.08~2.04 (m, 4H), 1.43~1.38 (m, 8H), 1.31~1.24 (m, J = Hz, 28H), 0.88~0.86 (t, J = 6.85 Hz, 6H).

II - ii -3. Measurement

^1H spectra were recorded on a JEOL JNM ECP-600 instrument with CD_3OD as the solvent. The thickness of the ZnO and the active layer were measured using an Alpha-Step IQ surface profiler (KLA-Tencor Co.). Kelvin probe microscopy (KPM) measurements were performed using KP technology Ltd. Model KP020 to measure the contact potential difference using KPM and investigate the effective work function of the substrate of the samples. The work function of the samples was estimated by the contact potential difference between the sample and the KPM tip. The KPM tip was calibrated against a standard reference gold surface, with a work function of 5.1 eV. The samples of **TEG-M-OTs** and **V-C12-OTs** were prepared by spin-coating them on ITO/ZnO and ITO surface using a methanol solution (1 mg/mL) at ambient condition, respectively. The current density-voltage measurements were performed under simulated light (AM 1.5G, 1.0 sun condition/100 mW/cm²) from a 150 W Xe lamp, using a KEITHLEY Model 2400 source measure unit. A calibrated Si reference cell with a KG5 filter certified by the National Institute of Advanced Industrial Science and Technology was used to confirm 1.0 sun condition.

II - ii -4. Fabrication of OSCs

The inverted type OSCs were fabricated with the structure [ITO/with or without ZnO(25nm)/**TEG-M-OTs** and **V-C12-OTs**(~5nm)/PTB7:PC₇₁BM(80nm)/MoO₃(3nm)/Ag(100nm)] and [ITO/ZnO(25nm)/MeOH/PTB7:PC₇₁BM(80nm)/MoO₃(3nm)/Ag(100nm)] for reference. A ZnO precursor was spin-coating on the pre-cleaned ITO substrate by the sol-gel process at 4000 rpm for 1 min. to a thickness of 25 nm, in which the sol-gel solution was prepared stirring zinc acetate dehydrate (0.100 g) and ethanolamine (0.025 ml) dissolved in 2-methoxyethanol (1 ml) at 60 °C for overnight. Then, the thin film of the ZnO precursor cured at 200 °C for 10 min. A thin layer of TEG-M-OTs and V-C12-OTs was prepared by spin coating with a MeOH solution of TEG-M-OTs and V-C12-OTs (1 mg/mL) at 4000 rpm for 1min onto the ITO or ZnO. The typical thickness was less than 5 nm. The active layer was spin-cast from a mixture of PTB7 and PC₇₁BM in which the mixture was prepared stirring PTB7 (10mg) and PC₇₁BM (15 mg) in 1 mL of chlorobenzene with 3% (v/v) 1,8-diiodooctane (DIO) at 1800 rpm for 120 s. The active solution was then filtered through a 0.2 µm membrane filter before spin coating. Finally, MoO₃ (3 nm) and Ag (100 nm) were thermally evaporated at 2×10^{-6} Torr. The device area was 12 mm².

II - iii Results and discussion

The positive effect as electrolyte based on tosylate anion have been reported, which is generated from the formation of hydrogen bonds between the OH groups of the alcoholic solvent and sulfonate group of tosylate anion.^[22] To investigate the effect of ETL on photovoltaic properties, the OSCs were fabricated with ITO/ETL/PTB7:PC₇₁BM/MoO₃/Ag, where **TEG-M-OTs** and **V-C12-OTs** were used as the ETL with or without ZnO as shown in **Fig. II-1**.

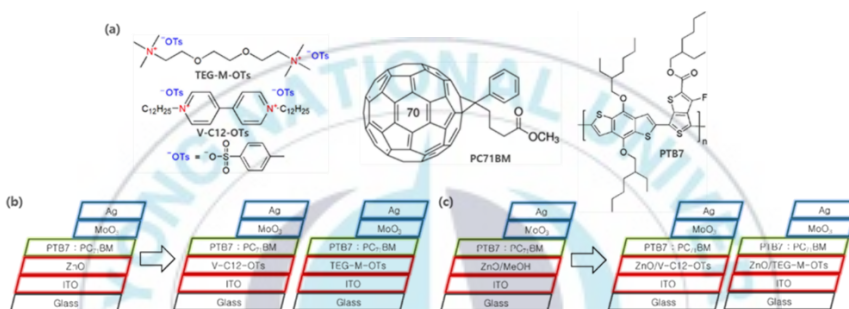


Figure II-1 Chemical structures of (a) TEG-M-OTs, V-C12-OTs, PC₇₁BM, and PTB7. Device structures based on (b) ITO and (c) ITO/ZnO.

Table II-1. Summary of photovoltaic parameters of OSCs based on ZnO, ITO/TEG-M-OTs, and ITO/V-C12-OTs; best (average).

ETL	J_{sc} (mA/cm ²)	V_{oc} (V)	FF (%)	PCE (%)	Work Function (eV)	R_s ($\Omega \cdot cm^2$)
ZnO/MeOH	14.48 (14.37)	0.76 (0.76)	68.1 (67.7)	7.48 (7.39)	4.36	2.81
ZnO/TEG-M-OTs	14.41 (14.20)	0.76 (0.76)	70.7 (70.6)	7.74 (7.62)	4.03	2.86
TEG-M-OTs	14.44 (14.31)	0.51 (0.48)	57.2 (55.0)	4.22 (3.81)	4.19	4.35
ZnO/V-C12-OTs	14.84 (14.73)	0.76 (0.76)	69.9 (69.6)	7.88 (7.79)	4.25	3.14
V-C12-OTs	14.66 (14.71)	0.71 (0.70)	66.7 (65.4)	6.95 (6.77)	4.29	3.12

The current density-voltage (J-V) characteristics of the OSCs under the

illumination and dark conditions are shown in **Fig. II-2** and their photovoltaic parameters are summarized in **Table 1**. The optimized device based on ZnO/V-C12-OTs showed the PCE up to 7.88% with a short circuit current density (J_{SC}) of 14.48 mA/cm², an open circuit voltage (V_{OC}) of 0.76V, and a fill factor of 69.9%. Though ZnO/TEG-M-OTs based device exhibited a similar V_{OC} value, the PCE is slightly lower than ZnO/V-C12-OTs due to the lower J_{SC} . This coincides that the leakage current of the device based on ZnO/TEG-M-OTs is much higher than that of the device of ZnO/V-C12-OTs. However, both devices based on ZnO/SM electrolytes as the ETL have higher PCE than the device based on ZnO/MeOH. This result corresponds with the WF from KPM measurement. The WFs of ZnO/SM electrolytes are smaller than ZnO/MeOH, which suggests that the small energy barrier height at the interface between the electrodes and active layer can induce the high PCE from the reduction of a Schottky barrier (as depicted in **Fig. II-3**).

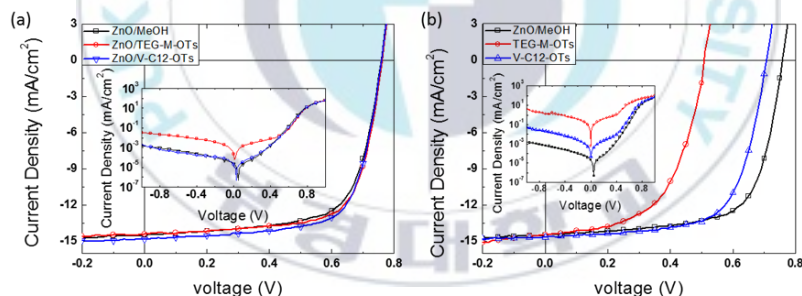


Figure II-2 Current-voltage curves of OSCs under AM 1.5G simulated illumination with an intensity of 100 mW/cm² (insert: in the dark condition; square: ZnO/MeOH, circle: TEG-M-OTs, triangle: V-C12-OTs) (a) with ZnO, and (b) without ZnO.

The performance of the ZnO-free device was also investigated by the same method. The best PCEs of the device based on TEG-M-OTs and V-C12-OTs showed up to 4.22 and 6.95%, which are lower than the values of the reference device (7.48%). The major loss of both ZnO-free devices was incurred from V_{OC} and FF. Also, the relationship between the PCE and the WF did not match exactly as mentioned before. These due to the large leakage current and the high

series resistance. Though the PCEs of devices based on SM electrolytes were not lower than that of the reference device (7.48%), it should be noted that the device based on **V-C12-OTs** showed the PCE near 7% without any calcination.

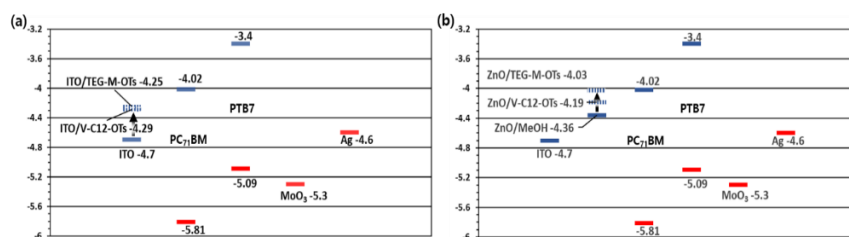
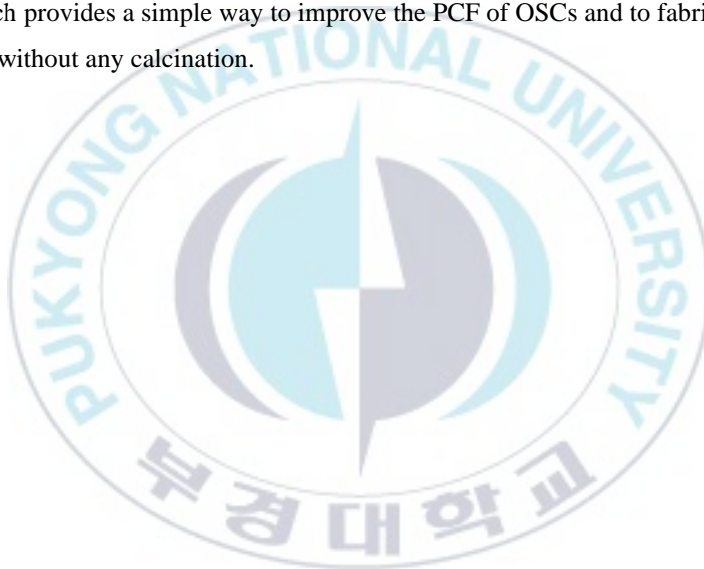


Figure II-3 The energy level diagram of the device based on (a) ITO/ZnO, (b) ITO.

II - iv **Conclusion**

A series of new small molecules with tosylate anions have been successfully synthesized by a simple quaternization reaction. The addition of a thin layer of **TEG-M-OTs** and **V-C12-OTs** improved the PCE of the OSCs, which was induced by the reduction of a Schottky barrier. The result from the KPM measurement supported the relationship between the PCE and the reduction of a Schottky barrier. In addition, the device based on **V-C12-OTs** without ZnO shows the PCE of 6.95%, showing the potential of ZnO-free OSCs. This research provides a simple way to improve the PCF of OSCs and to fabricate the OSCs without any calcination.



Chapter III

Structural Effect of Viologen-Based Organic Electrolytes on the Photovoltaic Property as the Cathode Buffer Layer

III- i Introduction

In our previous work, we have reported on the effects of anion size^[23, 24] or hydroxyl group^[13] of the organic electrolytes on the photovoltaic properties. In addition, the alkyl chain-length effect of using viologen-based polymer dyes as the electron transporting layer was investigated in conventional organic solar cells (OSCs).^[23] The results suggest that longer alkyl chains are more effective than shorter chains for the fabrication of efficient OSCs. Viologen derivatives are well known as electrochromic dyes,^[23-25] which show very high electron affinity, high-lying reduction potential, and good solubility in water or alcoholic aqueous solvent. Thus, viologen derivatives can be applied to the ETL for OSCs. Based on our previous studies, as shown in **Fig.III-1(a)**, we designed and synthesized three types of small-molecule dyes with a structure of 1,10-bis(1-alkyl)-4,40-bipyridine-1,10-dium benzenesulfonate (**V-alkyl-OTs**) to investigate the effects of the alkyl chain length on the photovoltaic properties. The alkyl groups examined butyl, hexyl, and dodecyl, denoted as **C4**, **C6**, and **C12**, respectively. The magnitudes of the dipole moment of ionic compounds are proportional to the size of the compounds. Thus, the magnitudes of the dipole moments of **V-alkyl-OTs** structures will be in the order of **C4** < **C6** < **C12**. A longer alkyl chain can induce a larger dipole moment, even when the alkyl group is attached to the amino cation, there is a similar correlation between the alkyl chain length and the dipole moment.^[27-29] Therefore, a larger

dipole moment of **V-alkyl-OTs** further will reduce the energy offset at the electrode interface, especially between the electron transporting layer (ZnO) and the photoactive layer. However, an excessively long alkyl chain would reduce the PCE by generating the insulation region on the ETL. Thus, it is important to find out the appropriate length of the alkyl chain in a trade-off relationship between the dipole moment and electrical property of materials. Following this basic concept, we selected butyl (**C4**), hexyl (**C6**), and dodecyl (**C12**) as the alkyl groups and fabricated the OSCs with **V-alkyl-OTs** as the ETL. As illustrated in **Fig. III-1(b)**, the devices were fabricated with a configuration of ITO/ZnO/**V-alkyl-OTs**/PTB7:PC₇₁BM/MoO₃/Ag. The PCEs of the device with ZnO/**V-alkyl-OTs** were improved from 7.6% ($J_{SC} = 16.0 \text{ mA/cm}^2$, $V_{OC} = 0.72 \text{ V}$, FF = 65.6%) with pristine ZnO to 8.1% (**C4**, $J_{SC} = 16.8 \text{ mA/cm}^2$, $V_{OC} = 0.73 \text{ V}$, FF = 65.9%), 8.3% (**C6**, $J_{SC} = 17.2 \text{ mA/cm}^2$, $V_{OC} = 0.72 \text{ V}$, FF = 67.3%), and 8.6% (**C12**, $J_{SC} = 18.0 \text{ mA/cm}^2$, $V_{OC} = 0.72 \text{ V}$, FF = 66.4%). The enhancement of the PCE is strongly related to alkyl chain length, contributed mostly by the improvement of the J_{SC} due to the reduction in the energy offset at the cathode interface.

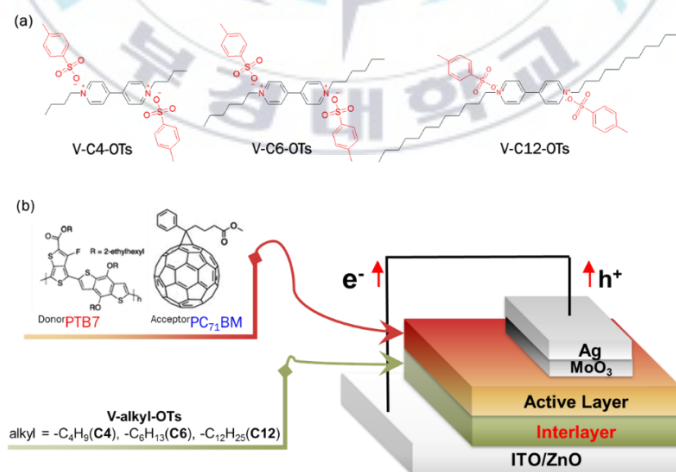


Figure III-1 Current density–voltage curves of OSCs ZnO, ZnO/V-alkyl-OTs under illumination (inset: in the dark condition) in this research.

III- ii Experiment

III- ii -1. Materials

All chemicals were purchased from Alfa Aesar or Sigma-Aldrich and used as received unless otherwise described. PTB7 (Poly({4,8-bis[(2-ethylhexyl)oxy]benzo[1,2-*b*:4,5-*b'*]dithiophene-2,6-diyl}{3-fluoro-2-[(2-ethylhexyl)carbonyl]thieno[3,4-*b*]thiophenediyl}))) and PC₇₁BM ([6,6]-phenyl C₇₁ butyric acid methyl ester) (Cat No. S2458) were purchased from 1-material Co. and Derthon optoelectronic materials science technology Co. LTD, respectively.



III- ii -2. Synthesis of V-Alkyl-OTs

1,1'-bis(1-butyl)-4,4'-bipyridine-1,1'-diium benzenesulfonate (V-C4-OTs).

A mixture of 4,4'-bipyridine (0.625 g, 4.00 mmol), and butyl 4-methylbenzenesulfonate (1.826 g, 8.00 mmol) in dimethylformamide was stirred at 70 °C for 1 day. After cooling down to room temperature, white precipitates (**V-C4-OTs**) were filtered and washed with copious amount of acetonitrile. The product yield was 89.7%. ESI-MASS (m/z) $[M-H]^+$ 613, $[M-Na]^+$ 635. 1H NMR (600 MHz, CD_3OD , ppm) δ 9.25~9.23 (d, J = 8.2 Hz, 4H), 8.64~8.62 (d, J = 7.6 Hz, 4H), 7.66~7.65 (d, J = 7.6 Hz, 4H), 7.21~7.20 (d, J = 7.6 Hz, 4H), 4.75~4.69 (t, J = 6.9 Hz, 4H), 2.38 (s, 6H), 2.05~2.03 (m, 4H), 1.45~1.43 (m, 4H), 1.03~1.00 (t, J = 6.5 Hz, 6H). ^{13}C NMR (150 MHz, CD_3OD , ppm) δ 149.88, 145.72, 142.32, 140.40, 128.54, 126.94, 125.59, 61.73, 33.10, 19.97, 19.13, 12.45. Anal. Calcd. For $C_{32}H_{40}N_2O_6S_2$: C, 62.72; H, 6.58; N, 4.57; S, 10.46. Found: C, 62.55; H, 6.41; N, 4.44; S, 10.38.

1,1'-bis(1-hexyl)-4,4'-bipyridine-1,1'-diium benzenesulfonate (V-C6-OTs).

A mixture of 4,4'-bipyridine (0.625 g, 4.00 mmol), and hexyl 4-methylbenzenesulfonate (2.051 g, 8.00 mmol) in dimethylformamide was stirred at 70 °C for 1 day. After cooling down to room temperature, white precipitates (**V-C6-OTs**) were filtered and washed with copious amount of acetonitrile. The product yield was 85.7%. ESI-MASS (m/z) $[M-H]^+$ 669, $[M-Na]^+$ 691. 1H NMR (600 MHz, CD_3OD , ppm) δ 9.18~9.14 (d, J = 7.6 Hz, 4H), 8.56~8.55 (d, J = 6.2 Hz, 4H), 7.61~7.58 (d, J = 8.3 Hz, 4H), 7.14~7.10 (d, J = 8.3 Hz, 4H), 4.64~4.61 (t, J = 7.6 Hz, 4H), 2.27 (s, 6H), 2.00~1.95 (m, 4H), 1.37~1.21 (m, 12H), 0.85~0.80 (t, J = 7.3 Hz, 6H). ^{13}C NMR (150 MHz, CD_3OD , ppm) δ 149.87, 145.72, 142.34, 140.40, 128.55, 126.94, 125.59, 61.73, 33.10, 30.56, 19.98, 19.13, 18.31, 12.46. Anal. Calcd. For $C_{36}H_{48}N_2O_6S_2$: C, 64.64; H, 7.23; N, 4.19; S, 9.59. Found: C, 64.55; H, 7.19; N, 4.08; S, 9.42.

1,1'-bis(1-dodecyl)-4,4'-bipyridine-1,1'-diium benzenesulfonate (V-C12-OTs). A mixture of 4,4'-bipyridine (0.625 g, 4.00 mmol), and 1-bromododecane

(1.993 g, 8.00 mmol) in dimethylformamide was stirred at 70 °C for 1 day. After cooling down to room temperature, white precipitates (**V-C12-Br**) were filtered and washed with copious amount of acetonitrile. Ion exchange reaction was proceed without purification. A solution of sodium 4-methylbenzenesulfonate (1.165 g, 6.00 mmol) in 10.0 mL deionized water was added dropwise in a solution of **V-C12-Br** (1.309 g, 2.00 mmol) in 10.0 mL of deionized water. After adding a solution of sodium 4-methylbenzenesulfonate (1.165 g, 6.00 mmol), the mixture was stirred at room temperature for 1 day. The white precipitates (**V-C12-OTs**) were filtered and washed with copious amount deionized water. The product yield was 85.6%. ESI-MASS (m/z) [$M-H$]⁺ 837, [$M-Na$]⁺ 859. ¹H NMR (600 MHz, CD₃OD, ppm) δ 9.25~9.24 (d, J = 6.2 Hz, 4H), 8.64~8.63 (d, J = 6.2 Hz, 4H), 7.67~7.66 (d, J = 8.2 Hz, 4H), 7.21~7.20 (d, J = 7.6 Hz, 4H), 4.72~4.69 (t, J = 7.5 Hz, 4H), 2.35~2.32 (t, 6H), 2.08~2.04 (m, 4H), 1.43~1.38 (m, 8H), 1.31~1.24 (m, 28H), 0.88~0.86 (t, J = 6.9 Hz, 6H). ¹³C NMR (150 MHz, CD₃OD, ppm) δ 151.49, 147.32, 143.95, 141.97, 130.15, 128.54, 127.21, 63.56, 33.35, 32.83, 31.02, 30.94, 30.81, 30.76, 30.45, 27.52, 24.02, 21.62, 14.73. Anal. Calcd. For C₄₈H₇₂N₂O₆S₂: C, 68.86; H, 8.67; N, 3.35; S, 7.66. Found: C, 68.77; H, 8.52; N, 3.23; S, 7.59.

III-ii -3. Measurement

^1H and ^{13}C NMR spectra were recorded on a JEOL JNM ECP-600 spectrometer. The thickness of the ZnO and the active layer were measured using an Alpha-Step IQ surface profiler (KLA-Tencor Co.). Static water contact angle images were captured after placing a 3 μL drop on the substrate and were performed using a contact angle measurement system (KRUS, Model DSA 100). Atomic force microscopy (AFM) images were captured using a Bruker (NanoScope V) AFM in the tapping mode. The water contact angles of the substrates were measured using KRUS Model DSA 100. Kelvin probe microscopy (KPM) measurements (KP technology Ltd. Model KP020) were performed to measure work function of ZnO layers with and without **V-C12-OTs**, **V-C6-OTs**, and **V-C4-OTs**, and the work function of the samples was estimated by measuring the contact potential difference between the sample and the KPM tip. The KPM tip was calibrated against a standard reference gold surface, with a work function of 5.1 eV. The current density-voltage measurements were performed under simulated light (AM 1.5G, 1.0 sun condition/100 mW/cm^2) from a 150 W Xe lamp, using a KEITHLEY Model 2400 source-measure unit. A calibrated Si reference cell with a KG5 filter certified by National Institute of Advanced Industrial Science and Technology was used to confirm 1.0 sun condition. Non-modulated impedance spectroscopy was performed using an impedance analyzer (WonATech., ZconTM Impedance Monitor) at an applied bias, 0V. A 50 mV voltage perturbation was applied over a constantly applied bias, 0 V, in the frequency range between 1 Hz and 1.0 MHz under the dark condition with the device for a Current density-Voltage (J-V) characteristics. The recombination resistances at an applied bias, 0V, deduced from equivalent circuit fitting.

III- ii -4. Fabrication of OSCs

In order to fabricate the inverted type organic photovoltaic (OPV) with the device structure: [ITO/ with or without ZnO(25nm)/each layer of **V-C12-OTs**, **V-C6-OTs**, and **V-C4-OTs**(~5nm)/active layer (PTB7 or PTB7-Th:PC₇₁BM, 70nm)/MoO₃(3nm)/Ag(100nm)], a ZnO layer was deposited on an ITO substrate by the sol-gel process. Zinc acetate dihydrate (0.1 g) and 0.025 mL of ethanolamine were dissolved in 1 mL of methoxyethanol and stirred at 60 °C for 12 hours under the air atmosphere. A thin film of ZnO sol-gel precursor was spin coated at 4000 rpm for 60 s then cured at 200 °C for 10 minutes. Each solution of **V-C12-OTs**, **V-C6-OTs**, and **V-C4-OTs** was spin coated on the ZnO layer at 4000 rpm for 60 s. The solution was prepared by using a concentration of 0.5 mg/ml in MeOH. For the thin layer on the ITO, the concentration of 1 mg/ml in MeOH. The last. The typical thickness of the layer was ~ 5 nm, which is measured using surface profiler and AFM. The active layer was spin-cast from a mixture of PTB7 and PC₇₁BM (obtained by dissolving 10 mg of PTB7 and 15 mg of PC₇₁BM in 1 mL of chlorobenzene with 3% (v/v) 1,8-diiodooctane (DIO)) and rotated at 1800 rpm for 120 s. The active solution was filtered through a 0.45 µm membrane filter before spin coating. Successive layers of MoO₃ and Ag were thermally evaporated through a shadow mask, with a device area of 0.09 cm² at 2 x 10⁻⁶ Torr.

II - ii -5. Fabrication of electron-only devices

Electron-only devices with the structure: [ITO/ZnO with each layer of **V-C12-OTs**, **V-C6-OTs**, and **V-C4-OTs**(30nm)/PC₇₁BM(60nm)/Al(100nm)], have been fabricated to investigate the electron mobility.



III-iii Results and discussion

III-iii-1 Characterization of V-alkyl-OTs and V-alkyl-OTs coated ZnO surface.

The chemical structures of the synthesized compounds were well characterized by the ^1H and ^{13}C NMR spectroscopy and elemental analysis. The ^1H NMR, ^{13}C NMR, ESI-MASS spectra of V-alkyl-OTs are showed in Fig. III-2.

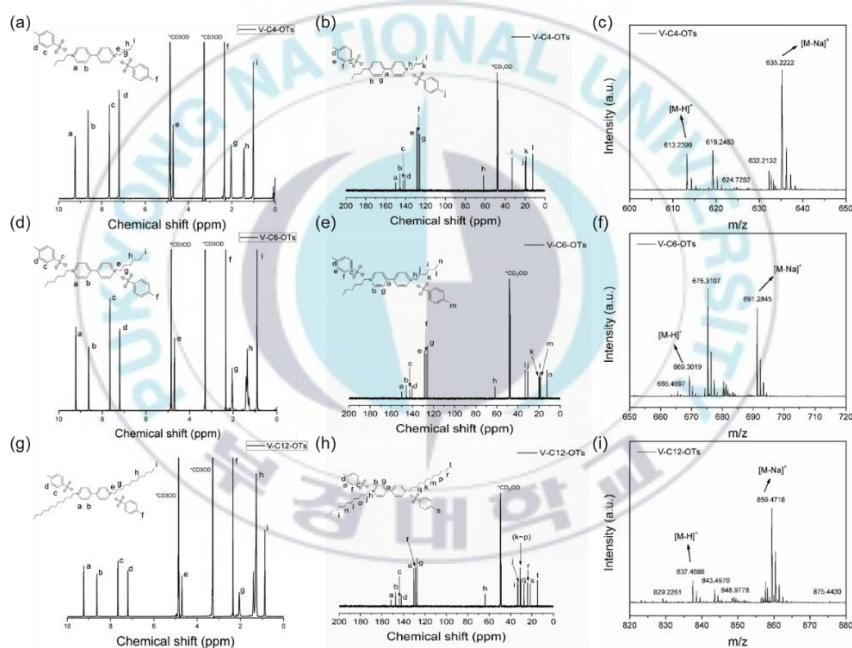


Figure III-2 ^1H NMR, ^{13}C NMR and electrospray ionization (ESI)-MASS spectra of V-alkyl-OTs; (a)-(c) C4, (d)-(f) C6, (g)-(i) C12.

To analyze the existence of V-alkyl-OTs on the surface of ZnO, we performed X-ray photoelectron spectroscopy (XPS) on the compounds. Fig. III-3 shows the XPS spectra of ZnO with and without V-alkyl-OTs. Signals at 400 and 167 eV correspond to N 1s and S 2p, respectively. Peaks at 1044 and 1021 eV in the XPS spectrum of ZnO correspond to Zn 2p_{1/2} and 2p_{3/2}, respectively. The

peaks in XPS spectra of ZnO with **V-alkyl-OTs** shifted toward higher energy because the Zn atoms become more electron-rich than in the ZnO without **V-alkyl-OTs**.

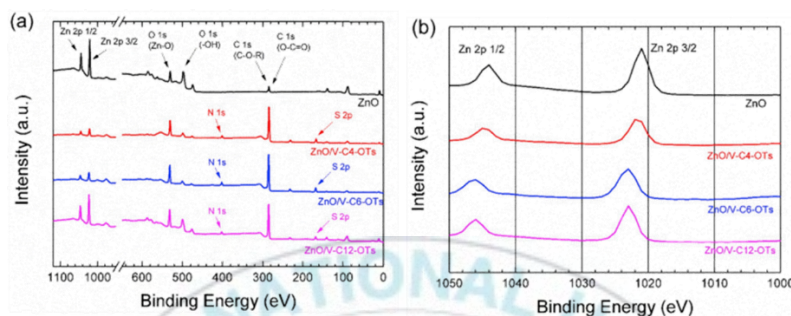


Figure III-3 (a) XPS survey spectra and (b) Zn 2p spectra of ZnO with and without **V-alkyl-OTs**.

The atomic force microscopy (AFM) images were observed of the **V-alkyl-OTs** treated ZnO layer (**Fig. III-4(a)**). The surface morphology of ZnO treated with **V-alkyl-OTs** was observed to be similar to the pristine ZnO. The average surface roughness (R_a) of **V-alkyl-OTs** with **C4**, **C6**, and **C12** measurements were 1.33, 1.37, and 1.47 nm, respectively. The water contact angle analysis (**Fig. III-5(b)**) was performed to investigate surface properties. Interestingly, the water contact angle of the **V-alkyl-OTs** coated ZnO layer gradually increased with increase in the alkyl chain length, 18.8° for **C4**, 21.1° for **C6**, and 21.6° for **C12**, which were smaller than the angle of pristine for the pristine ZnO surface (28.6°). This suggests that the ions of the electrolytes obviously reduce the water contact angle, but the ions would be shielded by the alkyl chain length.

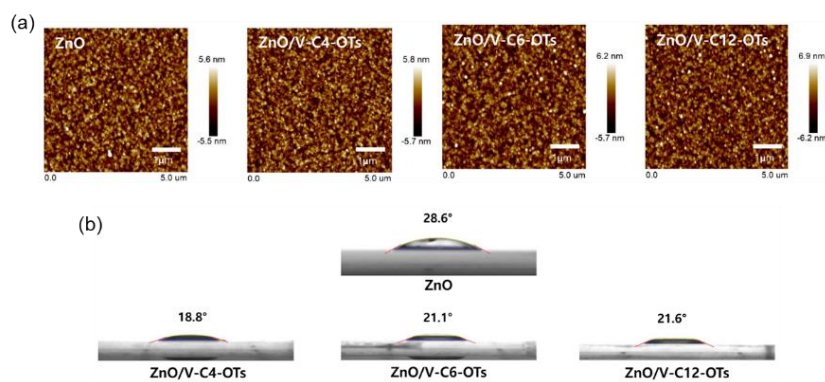
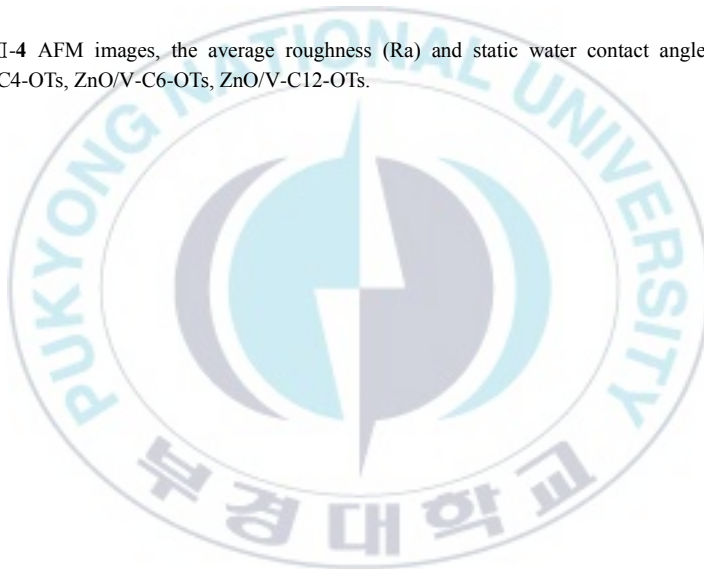


Figure III-4 AFM images, the average roughness (Ra) and static water contact angle of ZnO, ZnO/V-C4-OTs, ZnO/V-C6-OTs, ZnO/V-C12-OTs.



III-iii -2 Photovoltaic properties.

To demonstrate the effect of **V-alkyl-OTs** on the performance of the device, **V-alkyl-OTs** was used as the ETL in OSCs with the device configuration of ITO/ZnO/**V-alkyl-OTs**/PTB7:PC₇₁BM/MoO₃/Ag (shown in **Fig. III-1(b)**). The typical thickness of the **V-alkyl-OTs** layer was ~5 nm. **Fig. III-5(a)** shows the current density-voltage curves of OSCs with the **V-alkyl-OTs** layer as the ETL under illumination. The PCEs exhibited 8.1% (**C4**, $J_{SC} = 16.8 \text{ mA/cm}^2$, $V_{OC} = 0.73 \text{ V}$, FF = 65.9%), 8.3% (**C6**, $J_{SC} = 17.2 \text{ mA/cm}^2$, $V_{OC} = 0.72 \text{ V}$, FF = 67.3%), and 8.6% (**C12**, $J_{SC} = 18.0 \text{ mA/cm}^2$, $V_{OC} = 0.72 \text{ V}$, FF = 66.4%), which are greater than the results for the device with untreated-ZnO layer. (PCE = 7.6%, $J_{SC} = 16.0 \text{ mA/cm}^2$, $V_{OC} = 0.72 \text{ V}$, FF = 65.6%). Thus, a significant enhancement of 13.2% was observed in the device with the **V-C12-OTs** layer compared to the device with the untreated ZnO layer. The enhancement of J_{SC} was the main contribution to the PCE improvement. We performed the Kelvin probe microscopy (KPM) measurements to investigate the effect of **V-alkyl-OTs** on the J_{SC} . As mentioned before, the reduction of the energy offset at the interface is a crucial factor for a high J_{SC} because a large energy offset interrupts the charge collection.^[23, 30, 31] **Fig. III-5(b)** shows the energy diagram with the effective work function of the ZnO layer with and without **V-alkyl-OTs**. As shown in **Fig. III-5(b)**, the energy offset (ΔE) of the **V-alkyl-OTs** treated-ZnO surface exhibits 0.37 (**C4**), 0.30 (**C6**), and 0.23 (**C12**) eV, where the ΔE is defined as the difference between the LUMO of PC₇₁BM and the effective work function on the treated-ZnO surface. The values were smaller than that of the ZnO surface (0.44 eV) and the trend of ΔE is highly correlated to the length of the alkyl chain.

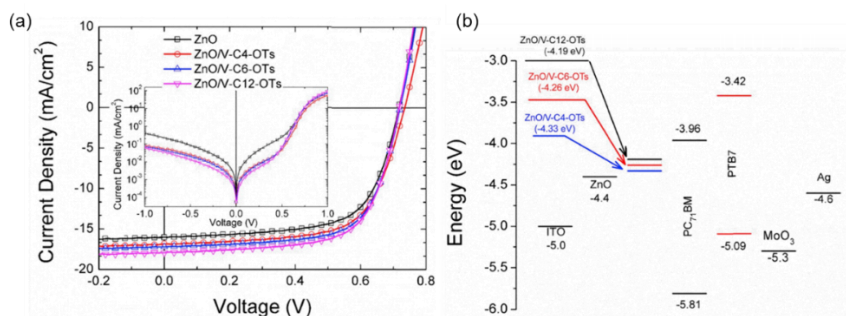


Figure III-5 (a) Current density–voltage curves of OSCs ZnO, ZnO/V-alkyl-OTs under illumination (inset: in the dark condition) and (b) the work function of ZnO/V-alkyl-OTs and the energy diagram of the device in this research.

Table III-1 Summary of photovoltaic parameters of OSCs based on ZnO, ITO/V-alkyl-OTs; best (average).

ETL	J_{sc} (mA/cm²)	V_{oc} (V)	FF (%)	PCE (%)	ΔE (eV)	R_s^a (Ω·cm²)
ZnO	16.0 (15.9)	0.72 (0.72)	65.6 (65.4)	7.6 (7.5)	0.44	2.81
ZnO/V-C4-OTs	16.8 (16.8)	0.73 (0.73)	65.9 (65.8)	8.1 (8.1)	0.37	2.86
ZnO/V-C6-OTs	17.2 (17.2)	0.72 (0.42)	67.3 (66.7)	8.3 (8.2)	0.30	4.35
ZnO/V-C12-OTs	18.0 (17.7)	0.72 (0.72)	66.4 (66.0)	8.6 (8.4)	0.23	3.12

To investigate the effect of **V-alkyl-OTs** on the electron collection capability, the electron-only devices with configurations of ITO/ZnO(25nm) **with** and **without** V-alkyl-OTs/PC₇₁BM(60nm)/Al(100nm) were fabricated and tested (**Fig. III-6(a)**). These devices exhibit a space charge limited current (SCLC) behavior above the built-in voltage, which is represented by the Mott-Gurney equation.^[32]

$$J = \frac{9}{8} \epsilon_0 \epsilon_r \mu \frac{E^2}{L}$$

where J is the current density, μ is the charge mobility, E is the electric field, $\epsilon_0 \epsilon_r$ is the permittivity of the active layer, and L is the thickness of the ZnO layer. Using $\epsilon_r = 3.9$ for PC₇₁BM to calculate the electron mobility. The electron mobility of the devices with **V-alkyl-OTs** were 2.43×10^3 (**C4**), 2.49×10^3 (**C6**), 2.89×10^3 (**C12**) cm² V⁻¹ s⁻¹, which are slightly higher values than the measured electron mobility of the ZnO layer without **V-alkyl-OTs** (2.24×10^3 cm² V⁻¹ s⁻¹). The trend of electron mobility data appeared to be correlated to the alkyl chain length of **V-alkyl-OTs**, but the change in electron mobility with **V-alkyl-OTs** is not significantly different from the value for the pristine ZnO. Similar features were found in the series resistance (R_s) data (**Table 1**). The R_s data of the devices with **V-alkyl-OTs** were almost similar to for the device based on pristine ZnO. However, the turn-on voltages of the devices with **V-alkyl-OTs** were 1.02 (**C4**), 0.91 (**C6**), and 0.73 V (**C12**), which are smaller than that of the device without **V-alkyl-OTs** (1.39 V). The turn-on voltage^[33] is strongly correlated with the electron collection capability at the interface. The results agree with the increase in the J_{SC} and the decrease in the energy offset at the interface.

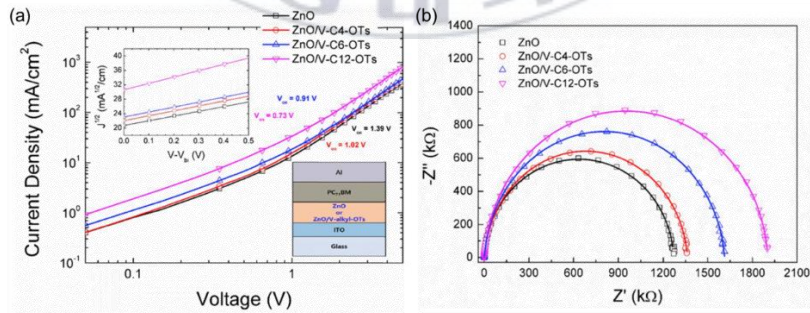


Figure III-6 (a) Current density–voltage curves of the electron-only device with a configuration of ITO/ZnO(25nm) with or without V-alkyl-OTs/PC₇₁BM(60nm)/Al(100nm). (inset: with fitted line, V : applied voltage, V_{bi} : built-in voltage, V_{on} : turn-on voltage) and **(b)** impedance spectra of the OSCs based on ZnO without and with V-alkyl-OTs.

Electronic impedance spectroscopy (EIS) was performed to investigate the carrier transport and recombination mechanism. The EIS spectra (**Fig. III-6(b)**) were linearly fitted to estimate the recombination resistance (R_{rec}). The larger EIS semi-circle reflects a greater recombination resistance. The higher R_{rec} values are related to the extraction of the charge at the ZnO interfaces. The R_{rec} of the devices with **V-alkyl-OTs** were 1360 (C4), 1650 (C6), 1950 (C12) k Ω , which are higher than the R_{rec} of the device with pristine ZnO (1230 k Ω). The results are consistent with the PCEs of the device

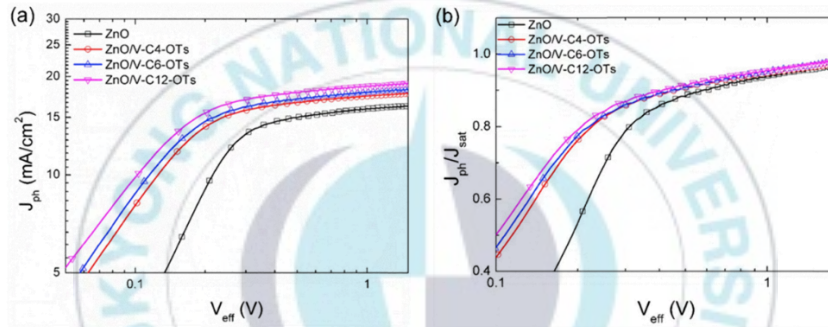


Figure III-7 (a) Photo-generated current density (J_{ph}) and (b) the carrier transporting and collecting probability vs. effective voltage (V_{eff}) plots of the OSCs.

In order to further understand the effect of **V-alkyl-OTs** on the charge transporting and collection properties, we plotted and analyzed the photocurrent density ($J_{\text{ph}} = J_{\text{L}} - J_{\text{D}}$) as a function of the effective voltage ($V_{\text{eff}} = V_0 - V_{\text{app}}$), where J_{L} is the current density under illumination, J_{D} is the current density under dark conditions, V_0 is the voltage at which $J_{\text{ph}} = 0$ and V_{app} is the applied voltage, respective. The voltages (V_{sat}) at which J_{ph} show the transition to the saturation regime were 0.275 V (ZnO), 0.199 V (ZnO/V-C4-OTs), 0.178 V (ZnO/V-C6-OTs), and 0.173 V (ZnO/V-C12-OTs) (shown in **Fig. III-7(a)**). Interestingly, the results strongly agree with the trend of the J_{SC} and the PCEs of the devices, because the small V_{sat} means the low energy barrier in the device. Using the carrier-transporting and collecting probability in the flat region of the J_{ph} from

the ratio of J_{ph}/J_{sat} can be estimated, where the J_{sat} is the saturated current density and calculated from the convergence value of J_{ph} . (**Fig.III-7(b)**) The carrier transporting and collecting probabilities at the J_{SC} condition were 93.17% (ZnO), 93.61% (ZnO/V-C4-OTs), 94.00% (ZnO/V-C6-OTs), 94.21% (ZnO/V-C12-OTs), respectively. Finally, the maximum exciton generation rate ($G_{max} = J_{ph}/(qL)$) at the V_{sat} , in which the q is the elementary charge and the L is the thickness of the active layer, was calculated as 1.141×10^{28} (ZnO), 1.254×10^{28} (ZnO/V-C4-OTs), 1.232×10^{28} (ZnO/V-C6-OTs), and 1.298×10^{28} (ZnO/V-C12-OTs) $m^{-3} s^{-1}$, respectively. No apparent changes were observed in G_{max} because the G_{max} correlates with the absorbance of the active layer. As mentioned before, the tendency of V_{sat} and the carrier transporting and collecting probability agrees with the increase in J_{SC} and the decrease in the energy barrier. This correlation means that the devices with ZnO/V-alkyl-OTs exhibited a decreased charge recombination and an increased charge collection capability at the cathode interface along the dipole moment of the applied materials

III-iv Conclusion

A series of small-molecule dyes based on dialkyl viologen with different alkyl chain length have been synthesized and demonstrated as the ETL layer for OSCs to investigate the structural variation of interlayer materials. The PCEs of the device with **V-alkyl-OTs** as the ETL were 8.1 (**C4**), 8.3 (**C6**), and 8.6% (**C12**), respectively. These values are better than the PCE of the device with pristine ZnO (7.6%) due to the formation of the interface dipole at the cathode interface by the thin layer of **V-alkyl-OTs**. Also, we found that the PCEs of the OSCs depend on the alkyl chain length of interlayer materials because longer alkyl chain induces a larger interface dipole. Similarly, the work function of the ZnO layer with **V-alkyl-OTs** is exhibited to depend on the size of the cation part, indicating that a Schottky barrier can be tuned by the size of the cation part. The major significant contribution to the enhancement of the PCE was through the improvement of the J_{SC} due to the reduction of the energy offset at the cathode interface. From the results, a longer alkyl chain induces a larger interface dipole, and the enhancement of the PCE is strongly related to alkyl chain length

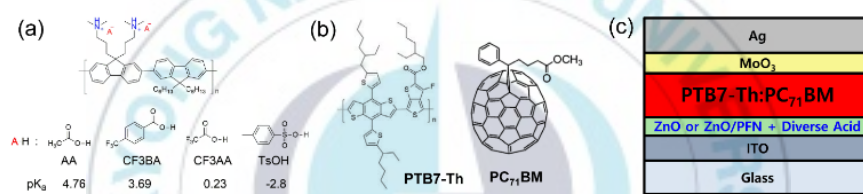
Chapter IV

Effect of acid derivatives with conjugated polymer electrolyte as the cathode buffer layer on the photovoltaic property

IV- i Introduction

Poly[(9,9-bis(3'-(N,N-dimethylamino)propyl)-2,7-fluorene)-alt-2,7-(9,9-dioctylfluorene)] (PFN) has been widely used in the electroluminescent devices^[34, 35] as the emitter and ETL for OSCs when compared with the other CPEs.^[36-39] This polymer can be dissolved in common solvents such as chlorinated hydrocarbon, tetrahydrofuran (THF), toluene, or xylene. Therefore, it is difficult to construct multi-layer structured devices because of the poor solvent resistance of the successive layer coating. However, quaternarizing the PFN with alkyl bromide (bromoethane or bromomethane) or adding a small amount of acetic acid (AA) to the PFN can alter the intrinsic solubility. Both quaternarized PFN and PFN modified with AA were readily soluble in polar solvents such as methanol, ethanol, N,N-dimethylformamide, and dimethylsulfoxide. These treatments allow PFN to fabricate multi-layer structured devices. A typical degree of quaternarization for PFN is less than 90%^[34,39] even after a long quaternarization reaction time (a week or longer). PFN salts are easily formed by the simple acid-base reaction of AA with tertiary amine group in the side chain of PFN. These salts do not dissolve in chlorinated hydrocarbon, THF, toluene, or xylene. Therefore, adding AA in the PFN matrix is convenient for preparing insoluble film with solvent resistance on the successive layer coating. However, it is necessary to systematically study the effect of the amount of added AA on the device performance because excess of

AA in the PFN layer can destroy the device. Polyelectrolytes with different counter anions have also been used to enhance the electron injection/collection ability at the cathode interface.^[23, 24, 32] Therefore, it is necessary to study the effect of the type of acid additives on the photovoltaic properties to understand the role of counter anion of acid derivatives. In this study, we report the photovoltaic properties of inverted OSCs (shown in **Fig.IV-1(b), (c)**) based on PFN with different amounts and types of acid derivatives (shown in **Fig.IV-1(a)**) as the ETL. To the best of our knowledge, the effect of the amount and type of acid additives in PFN interlayer on the photovoltaic properties have never been reported before.



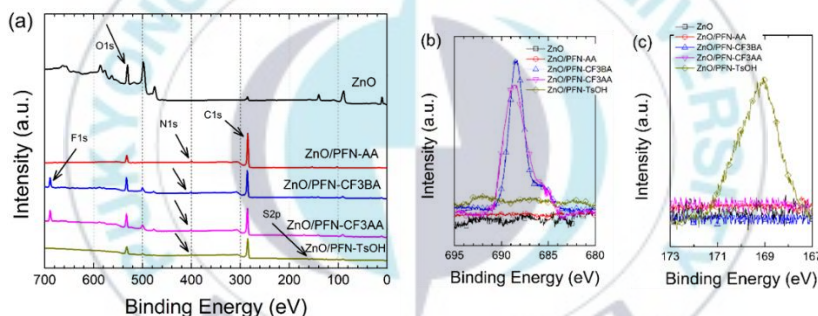
FigureIV-1 Chemical structure of **(a)** PFN with diverse acid derivatives, **(b)** PTB7-Th and PC₇₁BM, and **(c)** the device structure of OSC used in this study.

IV- ii Experiment

Materials. All chemicals were purchased from Alfa Aesar or Sigma-Aldrich and used as received unless otherwise described. Poly([2,6'-4,8-di(5-ethylhexylthienyl)benzo[1,2-b;3,3-b]dithiophene]{3-fluoro-2[(2-ethylhexyl)carbonyl]thieno[3,4-b]thiophenediy)}) (PTB7-Th) and PC₇₁BM ([6,6]-phenyl C71 butyric acid methyl ester) (Cat No. nano-cPCBM-SF) were purchased from 1-material Co., Derthon optoelectronic materials science technology Co. LTD, and nano-C, Inc., respectively. Poly[(9,9-bis(3'-(N,N-dimethylamino)propyl)-2,7-fluorene)-alt-2,7-(9,9-dihexylfluorene)] (PFN) was synthesized by the literature procedures.^[34, 35] And the rest part of experimental details, static water contact angle data, AFM images, IPCE spectra, and J-V curves of electron-only devices, and J_{ph} vs. V_{eff} curves of the devices are available in supporting information.

IV-iii Results and discussion

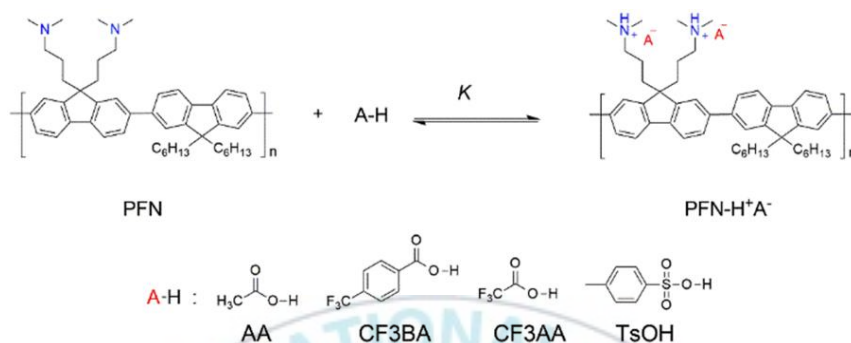
We used X-ray photoelectron spectroscopy (XPS) to analyze the presence of acid derivatives on the ZnO surface. **Fig.IV-2(a)** shows the survey spectra of acid derivatives on the ZnO surface. The peaks at 530, 400, and 285 eV in the survey spectra correspond to O 1s, N 1s, and C 1s, respectively. The peak at 688 eV in XPS spectra of ZnO/PFN-CF₃BA and ZnO/PFN-CF₃AA corresponds to F 1s (**Fig.IV-2(b)**). As shown in **Fig.IV-2(c)**, the peak at BE of 169 eV in the XPS spectrum of ZnO/PFN-TsOH corresponds to S 2p. The presence of the acid-base reaction product of PFN and acid derivatives was confirmed by the XPS spectra.



FigureIV-2 (a) XPS survey spectra, (b) F 1s, and (c) S 2p spectra of ZnO and PFN-acids coated ZnO.

The equilibrium constant (K) of the reaction between PFN and different types of acid derivatives (shown in **Fig.IV-3**) can be estimated by Poly[(9,9-bis(3'-(N,N-dimethylamino)propyl)-2,7-fluorene)-alt-2,7-(9,9-dioctylfluorene)] (PFN) where $pK_a (A - H)$ is the pK_a value of acid derivative and $pK_a (PFN - H^+ A^-)$ is the pK_a value of $PFN - H^+$. Assuming that $PFN-H^+$ is equivalent to trialkylammonium salt and its pK_a value is 10.75, the K values of acid-base reaction between PFN and different types of acid derivatives were estimated as 1.0×10^6 , 1.2×10^7 , 3.3×10^{10} , and 3.6×10^{13} for AA, CF₃BA, CF₃AA, and TsOH, respectively. Thus, it was confirmed that all the trialkylamine in the side

chains were completely converted to trialkylammonium salt by the addition of acid derivatives such as **AA**, **CF₃BA**, **CF₃AA**, and **TsOH**.



FigureIV-3 Reaction between PFN and acid derivatives.

We fabricated the inverted type OSCs (ITO/ZnO/PFN with acid derivatives/PTB7-Th:PC₇₁BM/MoO₃/Ag) to investigate the effect of different types of acid derivatives on the photovoltaic properties. Several different amounts of acid derivatives ranging from 0.5-6.0 eq were tested to detect the optimum concentration of acid derivatives (see **TableIV-1**). We noticed that the devices with PFN added with 1.0 eq of acid derivative exhibited the highest PCE. As for **AA**, the amount of **AA** did not significantly affect the PCE of the devices. In addition, excess of **CF₃BA** and **TsOH** did not significantly affect the PCE. This is presumably because these acid derivatives are in solid state. However, the PCE of the devices with PFN added with 6.0 eq of acid derivative was excessively lower when compared with the other type of devices. As shown in **Fig.IV-4**, the surface roughness of ZnO/PFN with 6.0 eq of **CF₃AA** was 5.39 nm, which was excessively larger than that of ZnO/PFN with 1.0 eq of **CF₃AA** (3.02 nm). This is because an excess of liquid **CF₃AA** may deteriorate the ZnO layer.

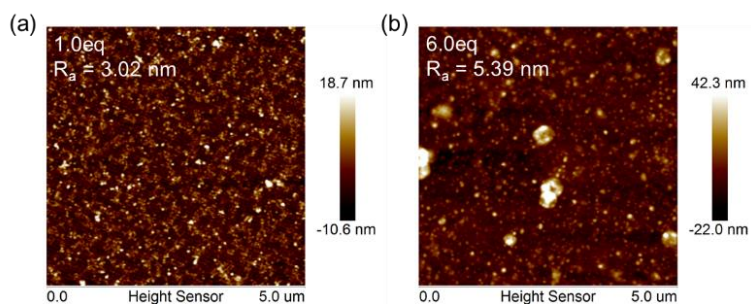


Figure IV-4 AFM images and the average roughness (R_a) of ZnO/PFN with (a) 1.0 eq and (b) 6.0 eq of CF₃AA.

Table IV-1 Summary of photovoltaic parameters of OSCs based on ZnO and ZnO/PFN with acid derivatives; best (average).

ETL	Amount of acid to PFN	J_{sc} (mA/cm ²)	V_{oc} (V)	FF (%)	PCE (%)	R_s^a (Ω cm ²)
ZnO		17.7 (17.5)	0.80 (0.80)	61.4 (60.9)	8.7 (8.5)	3.02
ZnO/PFN-AA	0.5 eq.	18.1 (18.0)	0.81 (0.80)	67.0 (66.9)	9.8 (9.6)	-
	1.0 eq.	18.8 (18.6)	0.80 (0.80)	66.5 (66.1)	9.9 (9.8)	2.64
	1.5 eq.	18.4 (18.3)	0.81 (0.80)	67.2 (66.4)	9.9 (9.8)	-
	6.0 eq.	18.2 (18.2)	0.80 (0.80)	66.8 (66.2)	9.7 (9.6)	-
ZnO/PFN-CF ₃ BA	0.5 eq.	18.7 (18.6)	0.81 (0.81)	68.2 (66.8)	10.3 (10.1)	-
	1.0 eq.	18.8 (18.7)	0.81 (0.80)	68.2 (67.4)	10.3 (10.1)	2.59
	1.5 eq.	18.3 (18.2)	0.80 (0.80)	61.5 (60.7)	9.0 (8.9)	-
	6.0 eq.	17.8 (17.7)	0.78 (0.78)	57.8 (57.6)	8.0 (7.9)	-
ZnO/PFN-CF ₃ AA	0.5 eq.	18.0 (17.8)	0.81 (0.81)	68.8 (68.0)	10.0 (9.8)	-
	1.0 eq.	18.4 (18.3)	0.81 (0.80)	69.5 (69.0)	10.3 (10.2)	2.48
	1.5 eq.	17.9 (17.8)	0.80 (0.79)	67.4 (67.0)	9.7 (9.5)	-
	6.0 eq.	15.0 (11.9)	0.39 (0.35)	21.6 (19.1)	1.3 (0.83)	-
ZnO/PFN-TsOH	0.5 eq.	18.5 (18.4)	0.81 (0.80)	68.3 (67.2)	10.2 (10.1)	-
	1.0 eq.	18.7 (18.6)	0.80 (0.80)	70.6 (69.7)	10.6 (10.4)	2.12
	1.5 eq.	18.2 (18.0)	0.81 (0.81)	67.6 (66.3)	9.9 (9.8)	-
	6.0 eq.	17.3 (17.2)	0.79 (0.79)	58.9 (56.8)	8.1 (7.7)	-

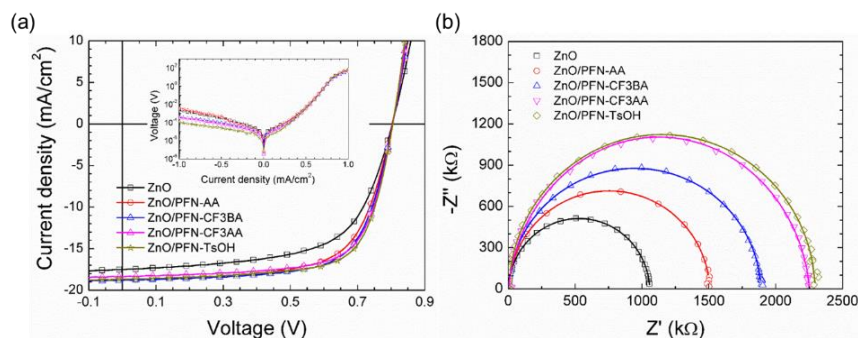
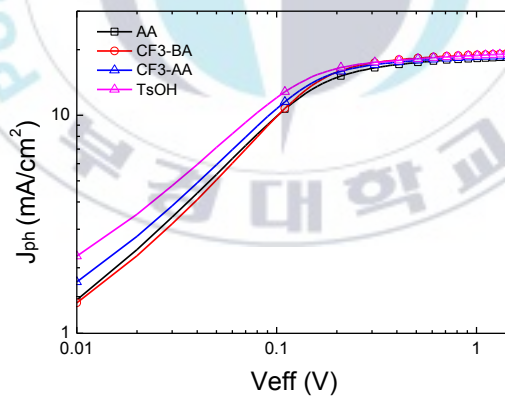


Figure IV-5 (a) Current density–voltage curves under illumination (inset: under dark conditions) and (b) EIS spectra of OSCs based on ZnO and ZnO/PFN with 1.0 eq of acid derivatives.

Fig. IV-5(a) displays the current density–voltage (J - V) curves of the OSCs with PFN added with an optimum amount of acid derivatives that exhibit the highest PCE under illumination (inset displays the J - V curves under dark conditions); their photovoltaic parameters are summarized in **Table IV-1**. The PCEs of the devices with AA, CF₃BA, CF₃AA, and TsOH were 9.9% ($J_{\text{SC}} = 18.8 \text{ mA}/\text{cm}^2$, $V_{\text{OC}} = 0.80 \text{ V}$, $\text{FF} = 66.5\%$), 10.3% ($J_{\text{SC}} = 18.8 \text{ mA}/\text{cm}^2$, $V_{\text{OC}} = 0.81 \text{ V}$, $\text{FF} = 68.2\%$), 10.3% ($J_{\text{SC}} = 18.4 \text{ mA}/\text{cm}^2$, $V_{\text{OC}} = 0.81 \text{ V}$, $\text{FF} = 69.5\%$), and 10.6% ($J_{\text{SC}} = 18.7 \text{ mA}/\text{cm}^2$, $V_{\text{OC}} = 0.80 \text{ V}$, $\text{FF} = 70.6\%$), respectively, whereas the PCE of the device with pristine ZnO was 8.7% with a $J_{\text{SC}} = 17.7 \text{ mA}/\text{cm}^2$, $V_{\text{OC}} = 0.80 \text{ V}$, and $\text{FF} = 61.4\%$. Thus, it is evident that a significant improvement can be obtained using the device based on ZnO/PFN with 1.0 eq of acid derivatives. The PCEs of the OSCs that are based on ZnO/PFN with 1.0 eq of AA, CF₃BA, CF₃AA, and TsOH were improved by 15.0, 18.9, 18.2, and 21.4%, respectively when compared with the OSC based on pristine ZnO. Interestingly, the performances of the devices follow the trend of the pK_{a} value of acid derivatives. The trend of J_{SC} data is not significantly dependent on the type of acid derivatives. The FFs of the OSCs with ZnO/PFN-AA (1.0 eq.), ZnO/PFN-CF₃BA (1.0 eq.), ZnO/PFN-CF₃AA (1.0 eq.), and ZnO/PFN-TsOH (1.0 eq.) were 8.3, 11.1, 13.2 and 15.0%, respectively when compared with the OSC with pristine ZnO. The main contributing factor for the enhancement of efficiency

was the improvement of FF. The series resistance (R_s) was obtained from the J-V curves obtained under dark conditions. The R_s of the devices with ZnO/PFN-AA, ZnO/PFN-CF₃BA, ZnO/PFN-CF₃AA, and ZnO/PFN-TsOH were 2.64, 2.59, 2.48, and 2.12 $\Omega \text{ cm}^2$, respectively, and these are smaller than that of the device with ZnO (3.02 $\Omega \text{ cm}^2$). The obtained R_s data support the trends of FF and PCE. To observe the carrier recombination and transport mechanism, we acquired the electrical impedance spectra (EIS) of the OSCs with ZnO and ZnO/PFN with 1.0 eq of AA, CF₃BA, CF₃AA, and TsOH, respectively under dark conditions. As shown in **Fig.IV-5(b)**, the EIS has been fitted linearly to analyze the recombination resistance (R_{rec}). The size of EIS semi-circle indicates the extent of R_{rec} . Thus, the magnitude of R_{rec} of the devices were in the order: ZnO (1150 k Ω) < ZnO/PFN-AA (1490 k Ω) < ZnO/PFN-CF₃BA (1890 k Ω) < ZnO/PFN-CF₃AA (2350k Ω) < ZnO/PFN-TsOH (2365k Ω); this can be related well with the FFs and PCEs of the OSCs.



FigureIV-6 The photocurrent density-effective voltage ($J_{\text{ph}}\text{-}V_{\text{eff}}$) plot of OSCs based on ZnO/PFN with 1.0 eq of acid derivatives.

Table IV-2 Summary of the photocurrent density-effective voltage (J_{ph} - V_{eff}) plot of OSCs.

	V_{sat} (V)	J_{ph}/J_{sat} at J_{SC} (%)	G at J_{SC} ($m^{-3} s^{-1}$)
ZnO/PFN-AA	0.180	0.941	1.61×10^{28}
ZnO/PFN-CF ₃ -BA	0.18	0.945	1.68×10^{28}
ZnO/PFN-CF ₃ -AA	0.16	0.949	1.64×10^{28}
ZnO/PFN-TsOH	0.15	0.952	1.66×10^{28}

Further, we evaluated the relationship between the photocurrent density (J_{ph}) and effective voltage (V_{eff}) to realize the charge transporting and collection properties of the devices. The J_{ph} and V_{eff} can be defined as J_L (current density under illumination) – J_D (current density under dark conditions) and V_0 (voltage at $J_{ph} = 0$) – V_a (applied voltage), respectively. As shown in **Fig. IV-6**, the V_{eff} values at saturated photocurrent regime (V_{sat}) of the device based on ZnO/PFN with 1.0 eq of **AA**, **CF₃BA**, **CF₃AA**, and **TsOH** were 0.18, 0.18, 0.16, and 0.15 V, respectively. The change of V_{sat} is also not significantly dependent on the type of acid derivatives. Noticeably, the trend of saturated voltage agrees with the change of J_{SC} of the OSCs because a smaller saturated voltage indicates a faster transition from the space-charge-limited regime to the saturation regime. The carrier transporting and collecting probability (J_{ph}/J_{sat}) can be estimated in the saturated region of J_{ph} , where saturation current density (J_{sat}) is estimated from the convergent value of J_{ph} . The J_{ph}/J_{sat} values at the J_{SC} condition of the OSCs with ZnO/PFN with 1.0 eq of **AA**, **CF₃BA**, **CF₃AA**, and **TsOH** were 94.1, 94.5, 94.9, and 95.2%, respectively. The maximum exciton generation rate (G_{max}) was calculated by using the equation, $J_{ph}/(q \cdot L)$, where q and L are the electron charge and thickness of the active layer, respectively. G_{max} is related to the absorption of light of the active layer.^[40] The G_{max} at the J_{sat} condition of the devices based on ZnO/PFN with 1.0 eq of **AA**, **CF₃BA**, **CF₃AA**, and **TsOH** were 1.61×10^{28} , 1.68×10^{28} , 1.64×10^{28} , and 1.66×10^{28} , respectively. No significant changes in G_{max} were observed because the G_{max} is dependent on the absorbance of the active layer.

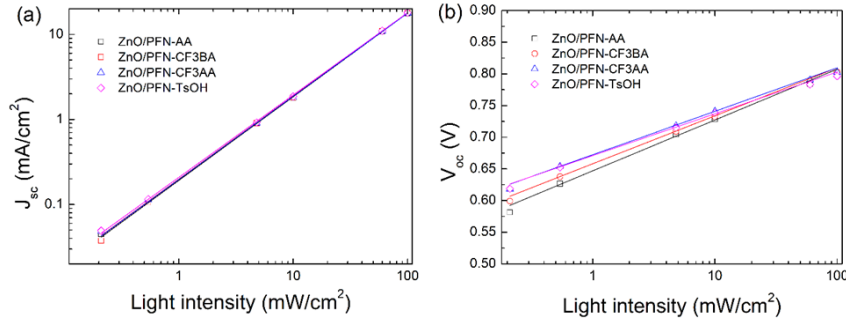


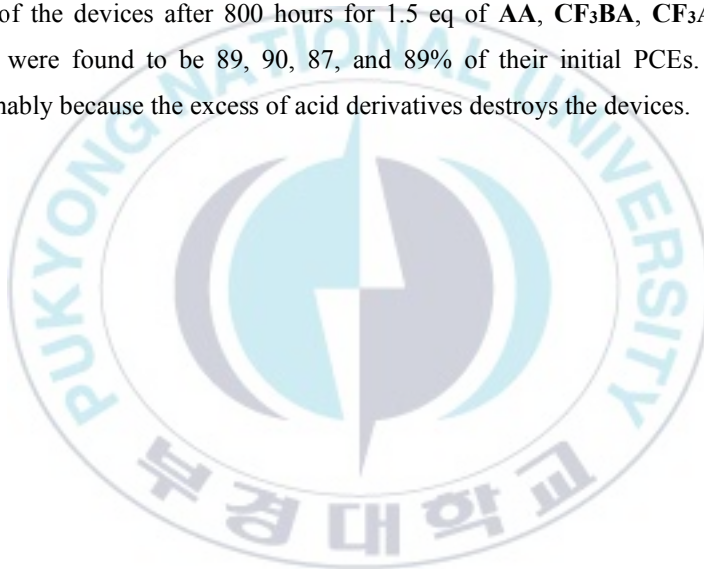
Figure IV-7 (a) J_{sc} and (b) V_{oc} vs. light intensity plots of the OSCs.

To realize the charge recombination kinetics at the interfaces further, we investigated the illumination intensity as a function of J_{sc} and V_{oc} of the devices.^[41–43] The relationship between J_{sc} and illumination intensity is generally defined by $J_{sc} \propto I^\alpha$, where I is the illumination intensity. When α is 1, the devices exhibit completely monomolecular recombination under short-circuit conditions. As shown in **Fig. IV-7(a)**, the α of the devices based on ZnO/PFN with 1.0 eq of **AA**, **CF₃BA**, **CF₃AA**, and **TsOH** were 0.98, 0.98, 0.98, and 0.97, respectively. This indicates that the devices exhibited slight bimolecular recombination because of the decreased space charge at the interfaces. However, the α values were not dependent on the type of acid derivatives. These results match well with the trend of J_{sc} and electron mobility of the devices. **Fig. IV-7(b)** displays V_{oc} as a function of illumination intensity.

The relationship between V_{oc} and illumination intensity is defined by $V_{oc} \propto (nkT/q)\ln(I)$, where k , T , and q are the Boltzmann constant, temperature in Kelvin, and electron charge, respectively. If the device has only the trap-assisted recombination channel, then the n value will be 2. If the device has only the band-to-band recombination, then the n value will be 1. The s values of the devices based on ZnO/PFN with 1.0 eq of **AA**, **CF₃BA**, **CF₃AA**, and **TsOH** were estimated to be 1.36, 1.28, 1.16, and 1.12, respectively from **Fig. 6(b)**. Thus, the devices exhibited reduced trap-assisted recombination. Note that the

change in s values of the devices agrees well with the trend of the PCEs of OSCs and follows the trend of the pK_a value of acid derivatives.

Furthermore, the devices were kept in a nitrogen-filled glove box without passivation. After 800 h, the PCEs of the devices based on ZnO/PFN with 1.0 eq of **AA**, **CF₃BA**, **CF₃AA**, and **TsOH** were found to be 97, 94, 97, and 96% of their initial PCEs. The acidity of the additives did not significantly affect device stability. However, the devices with excess acid derivatives exhibited poor stability when compared with the devices with 1.0 eq of acid derivatives. The PCEs of the devices after 800 hours for 1.5 eq of **AA**, **CF₃BA**, **CF₃AA**, and **TsOH** were found to be 89, 90, 87, and 89% of their initial PCEs. This is presumably because the excess of acid derivatives destroys the devices.



IV-iv Conclusion

To systematically study the effect of acid additives such as **AA**, **CF₃BA**, **CF₃AA**, and **TsOH** in PFN on the device performance, we fabricated and tested the inverted OSCs that use a blend of PTB7-Th and PC₇₁BM as the active layer and PFN with different amounts and types of acid derivatives as the ETL. The optimum amount of acid derivatives was found to be 1.0 eq for all the devices based on ZnO/PFN. The PCEs of the devices with 1.0 eq of **AA**, **CF₃BA**, **CF₃AA**, and **TsOH** were 9.9, 10.3, 10.3, and 10.6%, respectively, whereas the PCE of the device with pristine ZnO was 8.7%. The main contributing factor for the enhancement of PCE was the improvement of FF. The PCEs of the devices followed the trend of the acid dissociation constant of acid derivatives. We discovered that the most effective acid derivative was **TsOH** in this study. The devices based on PFN with acid derivatives exhibited reduced trap-assisted recombination and interfacial bimolecular recombination. Notably, reduced trap-assisted recombination of the devices agrees well with the trend of the PCEs of OSCs and follows the trend of the acid dissociation constant of acid derivatives.

References

- [1] S. I. Rasool, S. H. Schneider (1971), “Atmospheric Carbon Dioxide and Aerosols: Effects of Large Increases on Global Climate”, *Science*, 173, 3992, 138-141, *Science*.
- [2] J. S. SAWYER (1972), “Man-made Carbon Dioxide and the “Greenhouse” Effect”, *Nature*, 239, 23-26, *Nature*.
- [3] J. M. Barnola, D. Raynaud, Y. S. Korotkevich & C. Lorius (1987), “Vostok ice core provides 160,000-year record of atmospheric CO₂”, *Nature*, 329, 408-414, *Nature*.
- [4] IPCC (2014), “Climate Change 2014: Synthesis Report. Contribution of Working Groups I, II and III to the Fifth Assessment Report of the Intergovernmental Panel on Climate Change [Core Writing Team, R.K. Pachauri and L.A. Meyer (eds.)]. IPCC, Geneva, Switzerland.
- [5] G. Yu, J. Gao, J. C. Hummelen, F. Wudl, A. J. Heeger (1995), “Polymer Photovoltaic Cells: Enhanced Efficiencies via a Network of Internal Donor-Acceptor Heterojunctions”, *Science*, 270, 5243, 1789-1791, *Science*.
- [6] Yongye Liang, Zheng Xu, Jiangbin Xia, Szu-Ting Tsai, Yue Wu, Gang Li, Claire Ray, and Luping Yu (2010), “For the Bright Future—Bulk Heterojunction Polymer Solar Cells with Power Conversion Efficiency of 7.4%”, *Adv. Mater.*, 22, E135–E138, Wiley.
- [7] Wenchao Zhao, Deping Qian, Shaoqing Zhang, Sunsun Li, Olle Inganäs, Feng Gao, and Jianhui Hou (2016), “Fullerene-Free Polymer Solar Cells with over 11% Efficiency and Excellent Thermal Stability”, *Adv. Mater.*, 28, 4734–4739, Wiley.
- [8] Jun Yuan, Yunqiang Zhang, Liuyang Zhou, Guichuan Zhang, Hin-Lap Yip, Tsz-Ki Lau, Xinhui Lu, Can Zhu, Hongjian Peng, Paul A. Johnson, Mario Leclerc, Yong Cao, Jacek Ulanski, Yongfang Li and Yingping Zou¹ (2019), “Single-Junction Organic Solar Cell with over 15% Efficiency Using Fused-Ring Acceptor with Electron-Deficient Core”, *Joule*, 3, 1140–1151,

Elsevier.

- [9] Sean E. Shaheen, Christoph J. Brabec, and N. Serdar Sariciftci (2001), “2.5% efficient organic plastic solar cells”, *Appl. Phys. Lett.*, 78(6), 841 – 843, American Institute of Physics.
- [10] Jae Kwan Lee, Wan Li Ma, Christoph J. Brabec, Jonathan Yuen, Ji Sun Moon, Jin Young Kim, Kwanghee Lee, Guillermo C. Bazan, and Alan J. Heeger (2008), “Processing Additives for Improved Efficiency from Bulk Heterojunction Solar Cells”, *J. Am. Chem. Soc.*, 130, 3619-3623, American Chemical Society.
- [11] Chao He, Chengmei Zhong, Hongbin Wu, Renqiang Yang, Wei Yang, Fei Huang, Guillermo C. Bazan and Yong Cao (2010), “Origin of the enhanced open-circuit voltage in polymer solar cells via interfacial modification using conjugated polyelectrolytes”, *J. Mater. Chem.*, 20, 2617-2622, Royal Society of Chemistry.
- [12] Yuanbao Lin, Begimai Adilbekova, Yuliar Firdaus, Emre Yengel, Hendrik Faber, Muhammad Sajjad, Xiaopeng Zheng, Emre Yarali, Akmaral Seitkhan, Osman M. Bakr, Abdulrahman El-Labban, Udo Schwingenschlögl, Vincent Tung, Iain McCulloch, Frédéric Laquai, and Thomas D. Anthopoulos (2019), “17% Efficient Organic Solar Cells Based on Liquid Exfoliated WS₂ as a Replacement for PEDOT:PSS”, *Adv. Mater.*, 31, 1902965, Wiley.
- [13] Y.H. Kim, N. Sylvianti, M.A. Marsya, J. Park, Y.-C. Kang, D.K. Moon, J.H. Kim (2016), “A simple approach to fabricate an efficient inverted polymer solar cell with a novel small molecular electrolyte as the cathode buffer layer”, *ACS Appl. Mater. Interfaces.*, 8, 32992–32997, American Chemical Society.
- [14] S. Shao, K. Zheng, T. Pullerits, F. Zhang (2013), “Enhanced performance of inverted polymer solar cells by using poly(ethylene oxide)-modified ZnO as an electron transport layer”, *ACS Appl. Mater. Interfaces.*, 5, 380–385, American Chemical Society.

- [15] Y.H. Kim, D.G. Kim, R.D. Maduwu, H.C. Jin, D.K. Moon, J.H. Kim (2018), “Organic electrolytes doped ZnO layer as the electron transport layer for bulk heterojunction polymer solar cells”, *Sol. RRL.*, 2, 1800086, Wiley.
- [16] S. Nho, G. Baek, S. Park, B.R. Lee, M.J. Cha, D.C. Lim, J.H. Seo, S.-H. Oh, M.H. Song, S. Cho (2016), “Highly efficient inverted bulk-heterojunction solar cells with a gradiently-doped ZnO layer”, *Energy Environ. Sci.*, 9, 240–246, Royal Society of Chemistry.
- [17] S.-Y. Chang, Y.-C. Lin, P. Sun, Y.-T. Hsieh, L. Meng, S.-H. Bae, Y.-W. Su, W. Huang, C. Zhu, G. Li, K.-H. Wei, Y. Yang (2017), “High-efficiency organic tandem solar cells with effective transition metal chelates interconnecting layer”, *Sol. RRL.*, 1, 1700139, Wiley.
- [18] W. J. Potscavage Jr., S. Yoo, and B. Kippelen (2008), “Origin of the open-circuit voltage in multilayer heterojunction organic solar cells”, *Appl. Phys. Lett.*, 93, 193308, American Institute of Physics.
- [19] Erin L. Ratcliff, Andres Garcia, Sergio A. Paniagua, Sarah R. Cowan, Anthony J. Giordano, David S. Ginley, Seth R. Marder, Joseph J. Berry, Dana C. Olson (2013), “Investigating the Influence of Interfacial Contact Properties on Open Circuit Voltages in Organic Photovoltaic Performance: Work Function Versus Selectivity”, *Adv. Energy Mater.*, 3, 647–656, Wiley.
- [20] Wolfgang Tress, Karl Leo, Moritz Riede (2011), “Influence of Hole-Transport Layers and Donor Materials on Open-Circuit Voltage and Shape of I–V Curves of Organic Solar Cells”, *Adv. Funct. Mater.*, 21, 2140–2149, Wiley.
- [21] D. L. Mohle & G. Shen (2006), “The synthesis of tethered ligand dimers for PPAR γ –RXR protein heterodimers”, *Org. Biomol. Chem.*, 4, 2082–2087, Royal Society of Chemistry.
- [22] T. Y. Kim, J. E. Kim, K. S. Suh (2006), “Effects of alcoholic solvents on the conductivity of tosylate-doped poly(3,4-ethylenedioxythiophene)

- (PEDOT-OTs)", *Polym. Int.*, 55, 1, 80-86, Wiley.
- [23] M.Y. Jo, Y.E. Ha, J.H. Kim (2012), "Polyviologen derivatives as an interfacial layer in polymer solar cells", *Sol. Energy Mater. Sol. Cells*, 107, 1-8, Elsevier.
- [24] T.T. Do, H.S. Hong, Y.E. Ha, J. Park, Y-C Kang, J.H. Kim (2015), "Effect of polyelectrolyte electron collection layer counteranion on the properties of polymer solar cells." *ACS Appl. Mater. Interfaces*, 7, 3335-3341, American Chemical Society.
- [25] Roger J. Mortimer (1991), "Five color electrochromicity using prussian blue and nafion/methyl viologen layered films", *J. Electrochem. Soc.*, 138, 633-664, Electrochemical Society.
- [26] G.M. Ku, E. Lee, B. Kang, J.H. Lee, K. Cho, W.H. Lee (2017), "Relationship between the dipole moment of self-assembled monolayers incorporated in graphene transistors and device electrical stabilities", *RSC Adv.*, 7, 27100-27104, Royal Society of Chemistry.
- [27] H. Jin, B. O'Hare, J. Dong, S. Arzhantsev, G.A. Baker, J.F. Wishart, A.J. Benesi, M. Maroncelli (2018), "Physical properties of ionic liquids consisting of the 1-butyl-3-methylimidazolium cation with various anions and the bis (trifluoromethylsulfonyl)imide anion with various cations", *J. Phys. Chem. B*, 112, 81-92, American Chemical Society.
- [28] A.D.O. Cavalcante, M.C.C. Ribeiro, M.S. Skaf (2014), "Polarizability effects on the structure and dynamics of ionic liquids", *J. Chem. Phys.*, 140, 144108, American Institute of Physics.
- [29] Studzińska S, Molíková M, Kosobucki P, Jandera P, Buszewski B (2011), "Study of the interactions of ionic liquids in IC by QSRR", *Chromatographia*, 73, 35-44, Springer.
- [30] X. Jin, Y. Wang, X. Cheng, H. Zhou, L. Hu, Y. Zhou, L. Chen, and Y. Chen (2018), "Fluorine-induced self-doping and spatial conformation in alcohol-soluble interlayers for highly-efficient polymer solar cells" *J. Mater. Chem. A*, 6, 423-433, Royal Society of Chemistry.

- [31] D.G. Kim, Y.H. Kim, R.D. Maduwu, H.C. Jin, D.K. Moon, J.H. Kim (2018), “Organic electrolyte hybridized ZnO as the electron transport layer for inverted polymer solar cells. *J. Ind. Eng. Chem.*, 65, 175–179, Elsevier.
- [32] Anirban Baguiab, S. Sundar KumarIyerbc (2014), “Increase in hole mobility in poly (3-hexylthiophene-2,5-diyl) films annealed under electric field during the solvent drying step”, *Org. Electron.*, 15, 7, 1387–1395, Elsevier.
- [33] X. Guo, Y. Zhang, X. Liu, S. Braun, Z. Wang, B. Li, Y. Li, C. Duan, M. Fahlman, J. Tang, J. Fang, Q. Bao (2018), “Novel small-molecule zwitterionic electrolyte with ultralow work function as cathode modifier for inverted polymer solar cells”, *Org. Electron.*, 59, 15–20, Elsevier.
- [34] F. Huang, H. Wu, D. Wang, W. Yang, and Y. Cao (2004), “Novel Electroluminescent Conjugated Polyelectrolytes Based on Polyfluorene”, *Chem. Mater.*, 16, 708–716, American Chemical Society.
- [35] H. Wu, F. Huang, Y. Mo, W. Yang, D. Wang, J. Peng, and Y. Cao (2004), “Efficient Electron Injection from a Bilayer Cathode Consisting of Aluminum and Alcohol-/Water-Soluble Conjugated Polymers”, *Adv. Mater.*, 16, 1826–1830, Wiley.
- [36] Q. Sun, F. Zhang, J. Wang, Q. An, C. Zhao, L. Li, F. Teng and B. Hu (2015), “A two-step strategy to clarify the roles of a solution processed PFN interfacial layer in highly efficient polymer solar cells” *J. Mater. Chem. A*, 3, 18432–18441, Royal Society of Chemistry.
- [37] L. Zhang, C. He, J. Chen, P. Yuan, L. Huang, C. Zhang, W. Cai, Z. Liu and Y. Cao (2010), “Bulk-Heterojunction Solar Cells with Benzotriazole-Based Copolymers as Electron Donors: Largely Improved Photovoltaic Parameters by Using PFN/Al Bilayer Cathode”, *Macromolecules*, 43, 9771–9778, American Chemical Society.
- [38] T. Yang, M. Wang, C. Duan, X. Hu, L. Huang, J. Peng, F. Huang, and X. Gong (2012), “Inverted polymer solar cells with 8.4% efficiency by conjugated polyelectrolyte”, *Energy Environ. Sci.*, 5, 8208–8214, Royal

Society of Chemistry.

- [39] B. Liu, W.-L. Yu, Y.-H. Lai and W. Huang (2002), “Blue-Light-Emitting Cationic Water-Soluble Polyfluorene Derivatives with Tunable Quaternization Degree”, *Macromolecules*, 35, 4975–4982, American Chemical Society.
- [40] X. Jia, Z. Jiang, X. Chen, J. Zhou, L. Pan, F. Zhu, Z. Sun and S. Huang (2016), “Highly Efficient and Air Stable Inverted Polymer Solar Cells Using LiF-Modified ITO Cathode and MoO₃/AgAl Alloy Anode”, *ACS Appl. Mater. Interfaces*, 8, 3792–3799, American Chemical Society.
- [41] F. Yang, Y. Xu, M. Gu, S. Zhou, Y. Wang, K. Lu, Z. Liu, X. Ling, Z. Zhu, J. Chen, Z. Wu, Y. Zhang, Y. Xue, F. Li, J. Yuan and W. Ma (2018), “Synthesis of cesium-doped ZnO nanoparticles as an electron extraction layer for efficient PbS colloidal quantum dot solar cells”, *J. Mater. Chem. A*, 6, 17688–17697, Royal Society of Chemistry.
- [42] R. Azmi, S.-H. Oh and S.-Y. Jang (2016), “High-Efficiency Colloidal Quantum Dot Photovoltaic Devices Using Chemically Modified Heterojunctions”, *ACS Energy Lett.*, 1, 100–106, American Chemical Society.
- [43] L. J. A. Koster, V. D. Mihailetschi, R. Ramaker and P. W. M. Blom (2005), “Light intensity dependence of open-circuit voltage of polymer:fullerene solar cells”, *Appl. Phys. Lett.*, 86, 123509, American Institute of Physics.

Acknowledgement

참으로 짧은 기간이었지만 모든 성취를 떠나 대학원에 진학하여 만날 수 있었던 수많은 인연만을 생각하더라도 하나도 아쉽지 않은 결정이었습니다. 그만큼 소중한 사람들이 많고 감사의 말을 드리고 싶은 분들도 많습니다.

여러모로 부족한 저를 여기까지 이끌어 주신 **김주현 교수님**께 깊이 감사드립니다. 교수님의 좋은 가르침들을 완벽하게 따라가지 못했지만, 교수님의 기억에 갇혔던 학생으로 남았으면 합니다. 그리고 학부 때부터 지금까지 많은 도움을 주신 고분자공학과 교수님들께도 감사드립니다.

첫 연구실 생활에 적응하는데 큰 도움을 주신 우리 **윤환이형**과 **동근이형**, 없었으면 큰일났을 정도로 도와준 **미진이**, 잘 모르는 부분에서 항상 도와준 **준호**, 부족한 영어를 도와주던 야행성 **라트나**와 아이엠뷰티풀 **사브리나**, 마지막으로 가끔 진짜 어른 같은 **동환이** 등 짧은 연구실 생활에서 많은 소중한 사람들을 식구로 만난 덕분에 행복했습니다.

항상 제 선택을 지지해주는 **부모님**과 **동생**, 언제부터 만난지 모르겠는데 서로 놀려도 힘이 되는 **진욱이** **경록이** **상우**, 웃음이 멈추는 날이 없게 해준 만병 **지원이** 암아버네너 **연화** 어니언손 **동환이**, 학부부터 벌써 7년째인 항상 오랜만인 **민웅** 우리의 할배 **준성이형** 등 미처 언급하지 못한 모든 분들께도 무한한 감사의 말씀 전합니다. 덕분에 행복했습니다. 감사합니다.

2020년 02월

진호철 올림